High-resolution tractography protocol to investigate the pathways between human mediodorsal thalamic nucleus and prefrontal cortex

Abbreviated Title: Human mediodorsal nucleus thalamocortical tracts

Keywords: Thalamus; Thalamocortical; Diffusion MRI; Tractography; Reproducibility.

Authors: Liu Mengxing (刘梦醒)[1*], Garikoitz Lerma-Usabiaga[1,2], Francisco Clascá[3±] & Pedro M. Paz-Alonso[1,2*±]

Institutions: (1) BCBL. Basque Center on Cognition, Brain and Language, Donostia-San Sebastián, 20009, Spain.

(2) Ikerbasque, Basque Foundation for Science, Bilbao, 48013, Spain.

(3) Department of Anatomy and Neuroscience, School of Medicine, Autónoma de Madrid University, Madrid, 28029 Spain.

[*]Correspondence: Dr. Liu Mengxing / Dr. Pedro M. Paz-Alonso

BCBL, Paseo Mikeletegi 69, 2, 20009 Donostia-San Sebastián, Spain;

Tel: +(34) 943309300; E-mails: l.mengxing@bcbl.eu, kepa.pazalonso@gmail.com

[±]F.C. and P.M.P-A. share senior authorship

Number of Figures = 12.

Word count: Abstract = 230 words; Introduction = 705 words; Discussion = 1791 words.

Conflict of interest: The authors declare no competing financial interests.

Acknowledgements and Funding: The authors thank Caroline Handley for proofreading and helpful comments on the manuscript. L.M. was supported by grants from the European Union's Horizon 2020 research and innovation programme under the Marie Sklodowska-Curie (grant agreement No. 713673) and from "la Caixa" Foundation (grant no. 11660016 and grant no. 100010434 under the agreement no. HR18-00178-DYSTHAL). G.L-U. was supported by grants from the Spanish Ministry of Science and Innovation (IJC2020-042887-I and PID2021-123577NA-I00) and Basque Government (PIBA-2022-1-0014); F.C. was supported by grants from the Spanish Ministry of Science and Innovation (MICINN-AEI PCI2019-111900-2, PID2020-115780GB-I00); P.M.P-A. was supported by grants from the Spanish Ministry of Science and Innovation (PID2021-123574NB-I00), from the Basque Government (PIBA-2021-1-0003) and from the Red guipuzcoana de Ciencia, Tecnología e Innovación of the Diputación Foral de Gipuzkoa (FA/OF 422/2022), and 'La Caixa' Foundation (grant no. 100010434 under the agreement no. HR18-00178-DYSTHAL). BCBL acknowledges funding from the Basque Government through the BERC 2022-2025 program and by the Spanish State Research Agency through BCBL Severo Ochoa excellence accreditation CEX2020-001010-S.

Abstract

Animal studies have established that the mediodorsal nucleus (MD) of the thalamus is heavily and reciprocally connected with all areas of the prefrontal cortex (PFC). In humans, however, these connections are difficult to investigate. High resolution imaging protocols capable of reliably tracing the axonal tracts linking the human MD with each of the PFC areas may thus be key to advance our understanding of variation, development and plastic changes of these important circuits, in health and disease. Here, we tested in adult female and male humans the reliability of a new reconstruction protocol based on *in vivo* diffusion MRI to trace, measure and characterize the fiber tracts interconnecting the MD with 39 human PFC areas per hemisphere. Our protocol comprised three components: a) defining regions-of-interest; b) preprocessing diffusion data; and, c) modeling white-matter tracts and tractometry. This analysis revealed largely separate PFC territories of reciprocal MD-PFC tracts bearing striking resemblance with the topographic layout observed in macaque connection-tracing studies. We then examined whether our protocol could reliably reconstruct each of these MD-PFC tracts and their profiles across test and retest sessions. Results revealed that this protocol was able to trace and measure, in both left and right hemispheres, the trajectories of these 39 area-specific axon bundles with good-to-excellent test-retest reproducibility. This protocol, which has been made publicly available, may be relevant for cognitive neuroscience and clinical studies of normal and abnormal PFC function, development and plasticity.

Significance statement

Reciprocal MD-PFC interactions are critical for complex human cognition and learning. Reliably tracing, measuring and characterizing MD-PFC white-matter tracts using high-resolution non-invasive methods is key to assess individual variation of these systems in humans. Here, we propose a high-resolution tractography protocol that reliably reconstructs 39 area-specific MD-PFC white-matter tracts per hemisphere and quantifies structural information from diffusion MRI data. This protocol revealed a detailed mapping of thalamocortical and corticothalamic MD-PFC tracts in four different PFC territories (dorsal, medial, orbital/frontal pole, inferior frontal) showing structural connections resembling those observed in tracing studies with macaques. Furthermore, our automated protocol revealed high test-retest reproducibility and is made publicly available, constituting a step forward in mapping human MD-PFC circuits in clinical and academic research.

Introduction

The thalamus is a key hub in the multiregional sensory, motor, cognitive and emotion networks of the forebrain. First-order relay nuclei of the thalamus feed the cerebral cortex with information from the sensory periphery and subcortical motor systems via highly ordered, point-to-point axons, with minimal divergence or collateral branching (Guillery, 1995; Acsady, 2022). However, thalamic functions are not limited to the accurate and modulable signal relay that characterizes first-order relay sensorimotor nuclei (Sherman and Guillery 2002; Clascá, 2022). In the so-called higher-order nuclei, thalamic neurons receive convergent cortical and subcortical inputs in diverse combinations (Acsady 2022). Higher-order nuclei cells may relay signals between cortical areas (Sherman and Guillery, 1996; Theyel et al., 2010); engage in recurrent patterns of activity able to flexibly modulate intra- and inter-areal functional connectivity (Saalmann et al., 2012; Parnaudeau et al., 2013; Schmitt et al., 2017; Eradath et al., 2021); and/or integrate diverse signal flows in a non-linear fashion (Groh et al., 2014; Acsady, 2022). Moreover, the higher-order nuclei neuron axons typically branch to target separate areas and may establish functionally different synapses (Rodriguez-Moreno et al., 2020; Clascá, 2022). Therefore, higher-order nuclei are in position to dynamically select or coordinate computations across spatially segregated but functionally related areas. Such functions are critical for higher cognitive functions (Halassa and Kastner, 2017).

The mediodorsal nucleus (MD) of the thalamus is one of the largest higher-order nuclei, characterized by its massive and reciprocal interconnections with the prefrontal cortex (PFC), both in humans and other mammals. In fact, the original concept of PFC is defined by some authors as the projection field of MD (Carlén, 2017). Studies in non-human primates (NHPs) (Preuss and Goldman-Rakic, 1987; Giguere and Goldman-Rakic, 1988; Barbas et al., 1991; Siwek and Pandya, 1991; Yeterian and Pandya, 1991; Ray and Price, 1993; Cavada et al., 2000; Erickson and Lewis 2004) have consistently shown that MD can be divided into three major cytoarchitectonic divisions, which each have specific reciprocal connections with different groups of PFC areas: the paralaminar/lateral MD connects with the frontal eye fields and premotor areas [including Brodmann area (BA) 8]; the parvicellular MD connects with the anterior dorsolateral, polar (BAs9, 46, 10) and

ventrolateral (BAs44, 45, 47) PFC areas; and the medial magnocellular MD connects reciprocally with the orbital and ventromedial PFC (BAs11, 13, 14, 12/47) areas. Overall, these separate MD-PFC relationships form three major networks, each with distinct roles in cognition and behavior. The general layout of these pathways seems to be similar in humans (Klein et al., 2010), although given the remarkable expansion and diversification of granular isocortical PFC areas in humans (Glasser et al., 2016; Carlén 2017; Preuss and Wise 2021) the area-specific wiring of MD-PFC connections remains largely uncharacterized.

Tractography is the most powerful non-invasive methodology to investigate white-matter long-range connections in the human brain. Previous studies have used tractography to examine the organization of MD-PFC circuits and the associations with clinical phenotypes (e.g., Long et al., 2017; Giraldo-Chica et al., 2018; Li et al., 2022). These studies either used coarse PFC segmentations (e.g., Klein et al., 2010; Giraldo-Chica et al., 2018; Li et al., 2022), or used diffusion tensor model procedures that do not consider fiber-crossing problems when reconstructing the extensive fiber bundles between MD and the whole PFC (e.g., Kito et al., 2009; Long et al., 2017). Developing and testing an accurate and reproducible ready-to-use protocol to reconstruct MD-PFC fiber bundles to infer the human brain structural connectivity holds much promise to unveil the involvement of these circuits in higher cognitive functions, as well as to examine clinical disorders such as schizophrenia and dyslexia.

To this end, we first defined protocol parameters to optimally reconstruct the white-matter tracts between MD and 39 PFC areas in both hemispheres using advanced tractography procedures, including: (I) fine-grained bundle segmentation; (II) state-of-the-art magnetic resonance imaging (MRI) protocols and tractography methods; (III) neuroanatomical validation; and (IV) automatization and reproducibility. Second, we tested the protocol in light of the known neuroanatomy in NHPs and its reproducibility by examining white-matter microstructural and macrostructural proxies between test and retest sessions, by, scanning a subset of participants using the same MRI protocol twice. We expect reproducibility to be high for the microstructural and macrostructural properties of these tracts, but to vary across tracts.

Methods

Participants

A total of 113 healthy volunteers (mean age = 24.5 years, SD = 4.33 years; 65 females) participated in the study. Twenty-four of the volunteers (mean age = 24.7 years, SD = 4.06 years; 13 females) returned for a second session in which they were scanned using the same MRI protocol (mean interval = 15 days, SD = 21.82 days, range: 7-104 days). All participants were right-handed and had normal or corrected-to-normal vision. No participant had a history of major medical, neurological, or psychiatric disorders. The study protocol was approved by the Ethics Committee of the Basque Center on Cognition, Brain and Language (BCBL) and was carried out in accordance with the Code of Ethics of the World Medical Association (Declaration of Helsinki) for experiments involving human participants. Prior to their inclusion in the study, all participants provided informed written consent. Participants received monetary compensation for their participation.

Data acquisition

Whole-brain MRI data acquisition was conducted on a 3-T Siemens Prisma Fit whole-body MRI scanner (Siemens Medical Solutions) using a 64-channel whole-head coil. The MRI acquisitions included one T1-weighted structural image (T1w) and Diffusion-Weighted Imaging (DWI) sequences. High-resolution MPRAGE T1-weighted structural images were collected with the following parameters: time-to-repetition (TR) = 2530 ms, time-to-echo (TE) = 2.36 ms, flip angle = 7°, field of view (FoV) = 256 mm, voxel size = 1 mm isotropic, 176 slices. In total, 100 diffusion-weighted images were acquired with an anterior to posterior phase-encoding direction and 50 isotropically distributed diffusion-encoding gradient directions. The 100 diffusion weighted images included 50 images with b-value of 1000 s/mm2 and 50 images with b-value of 2000 s/mm2. Twelve images with no diffusion weighting (b-value of 0 s/mm2) were obtained for motion correction and geometrical distortion correction, which comprised five images with the same phase-encoding direction as the DWI images and seven images with a reversed phase-encoding direction (posterior to anterior). Both DWI and b0 images shared the following parameters: TR = 3600 ms, TE = 73 ms, flip angle = 78°,

voxel size = 2 isotropic, 72 slices with no gap and a multiband acceleration factor of 3 (see also Liu et al., 2022).

Tractography pipeline

The tract reconstruction was conducted using the RTP2-pipeline (Lerma-Usabiaga et al., 2023), which guarantees data provenance and reproducibility. The RTP2-pipeline divides the process into ROI definition, DWI preprocessing, and tract identification and tractometry. The code and parameters are available through GitHub (github.com/MengxingLiu/Thatract2-paper) and Docker Hub (https://hub.docker.com/u/garikoitz). In total, 39 pairs of homogeneous white-matter tracts that connect MD with the prefrontal cortex were reconstructed bilaterally.

Region of interest (ROI) definition

Figure 1 shows an overview of the three main stages followed in the present work to obtain MD-PFC tracts. The crucial segmentation of the MD from the thalamus was performed using the segmentation of thalamic nuclei based on a probabilistic atlas of the human thalamus proposed by our group and colleagues (Iglesias et al., 2018), which is implemented in freesurfer (http://surfer.nmr.mgh.harvard.edu/). In this atlas, the MD has two subregions, medial MD and lateral MD, but we decided to combine them for tractography in the current work. This is more appropriate for our main objective, which was to characterize human white-matter tracts between the MD and the entire PFC. In addition, tracking these MD nuclei separately would have meant the use of small seeds, which is associated with reproducibility problems.

The PFC ROIs were obtained from the Human Connectome Project (HCP) atlas (Glasser et al., 2016) by transforming the atlas from MNI space to individual space using a non-linear transformation in ANTs (http://stnava.github.io/ANTs). The HCP atlas used a combination of cortical architecture, function, connectivity, and/or topography to delineate 180 areas across the cerebral cortex, providing a standardized and consistent framework for the segmentation of the PFC that is based on high-resolution neuroimaging data (i.e., highly detailed multimodal datasets from 210 subjects obtained through an automated parcellation pipeline), resulting in a detailed and accurate segmentation. This level of precision is particularly beneficial for studies like this one that involve

fine-grained analysis of specific brain regions or connectivity patterns. The fimbria was selected as an exclusion ROI to prevent tracking going posterior, and was defined by the amygdala segmentation implemented in freesurfer (Saygin et al., 2017). To make sure the ROIs extend to the interface of gray and white matter, all the ROIs in ROI#1 and ROI#2 were dilated by one voxel. The full parameter table can be found in the Github repository (https://github.com/MengxingLiu/THATRACT2_paper).

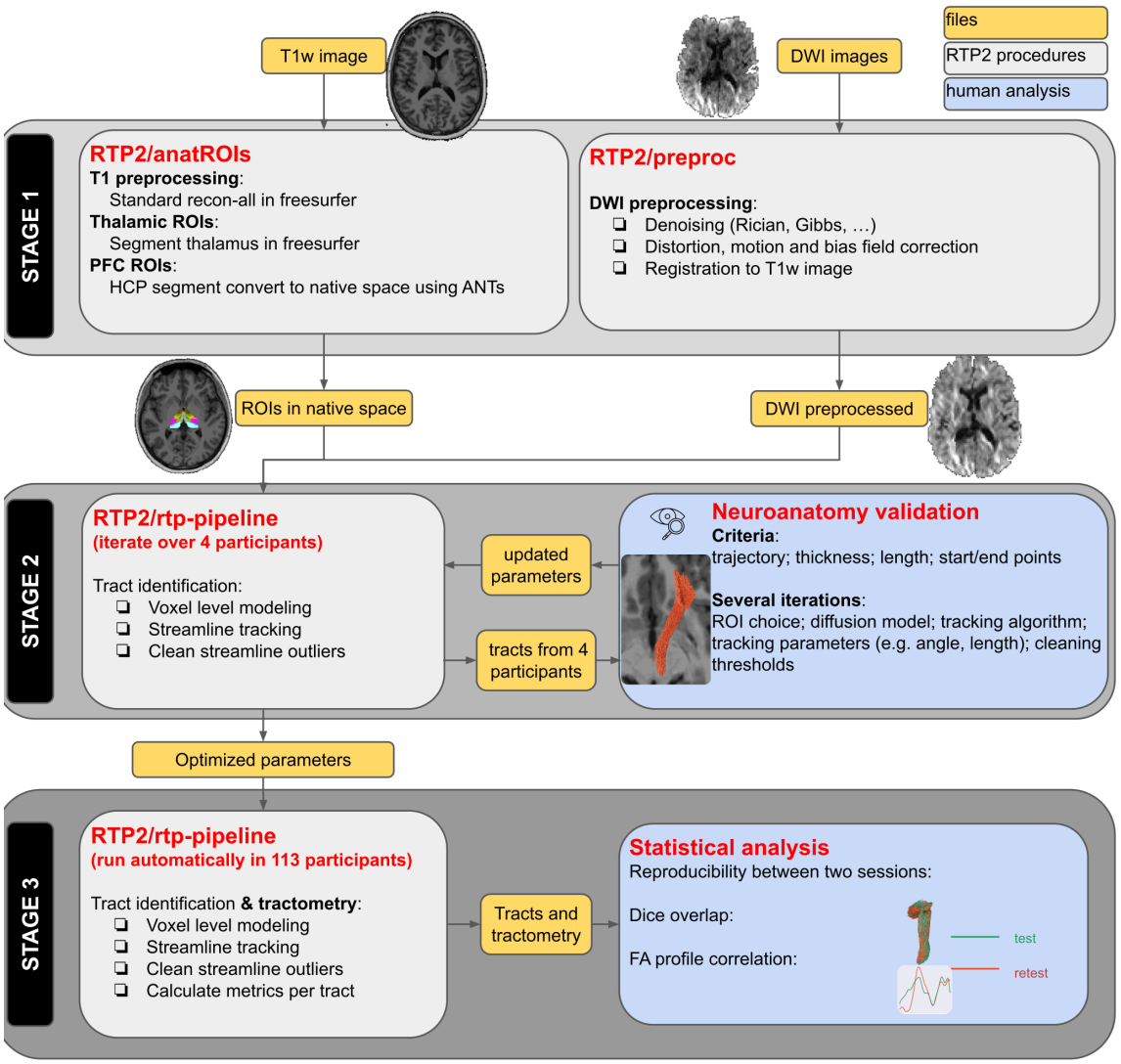

Figure 1. Overview of the three main stages involved in reconstructing the MD-PFC tracts in the present work, including RTP2 procedures and the MRI files used in each of them, as well as neuroanatomical validation (Stage 2) and statistical analysis (Stage 3).

Diffusion-weighted imaging (DWI) preprocessing

The preprocessing was conducted with RTP2-preproc (Figure 1, Stage 1). DWI preprocessing was mainly based on MRtrix's (Tournier et al., 2019) recommendations and used MRtrix tools, ANTs tool and FSL (Jenkinson et al., 2012). The data was preprocessed using several MRtrix functions in the following steps: 1) data denoising based on random matrix theory, which exploits data redundancy in the patch-level principal component analysis domain (Veraart et al., 2016) using *dwidenoise*; 2) Gibbs Ringing correction (Kellner et al., 2016) using *mrdegibbs*; 3) susceptibility induced distortions and motion correction with the FSL's topup and eddy tools (Smith et al., 2004) called by *dwifslpreproc*; 4) B1 field inhomogeneity correction with *dwibiascorrect* and Rician background noise removal with *mrcalc*; and 5) a rigid transformation matrix to align the DWI images to the corresponding T1w image using ANTs.

To make sure the DWI data from test and retest sessions were in the same space, DWI data from both sessions were aligned to the same T1w collected in the initial test session. Therefore, both test and retest sessions used the same ROIs; only DWI preprocessing and the streamline tracking were session-specific.

Tract identification and tractometry

The container RTP2-pipeline was used to obtain the final white-matter tracts. This container used the ROIs and the preprocessed DWI data to reconstruct the tracts of interest bilaterally and create the tractometry. We initially ran this step with 4 random participants and iterated multiple parameters. The optimal parameter combinations to identify each tract of interest were defined based on an expert anatomist's (FC) validation (Figure 1, Stage 2).

We first modeled the diffusion information at the voxel level to obtain a map of preferred directions with fiber orientation distributions (FODs). For this modeling we used MRtrix3's CSD algorithm (Jeurissen et al., 2014), as it can discern crossing fibers and provide more than one direction in each voxel. Next, streamline tractography was performed from the estimated FODs using MRtrix's iFOD2 algorithm (Tournier et al., 2010) with the following parameters: step size 1mm, FODs

amplitude threshold 0.05, angle threshold 45 degrees. The maximum and minimum fiber lengths vary across fiber groups, depending on their anatomical properties. Full details regarding length threshold for each fiber group are described in the GitHub repository (https://github.com/MengxingLiu/THATRACT2_paper), and can be adapted by future users of the tool to optimize them to their own data acquisition. Streamline generation was conducted bidirectionally (i.e., combining the streamlines obtained when seeding from ROI#1 to the target ROI#2, and in the opposite direction). Matlab utilities *AFQ_removeFiberOutliers* and *AFQ_ComputeTractProperties* developed in vistasoft (https://github.com/vistalab/vistasoft) were used to remove the outlier streamlines from each tract generated from MRtrix and to obtain the main tract metrics.

We generated tract profiles using the tract metrics obtained using vistasoft. CSD was used to model the fibers because of its ability to discern crossing fibers. Then classical DTI modeling was used to obtain the typical diffusion summary statistics, such as fractional anisotropy (FA), axial diffusivity, mean diffusivity and radial diffusivity. To generate the tract profiles, we obtained the central location of all the streamlines in the tract and sampled it into 100 same-length segments. The diffusion properties were summarized at each segment by taking a weighted average of the diffusion properties corresponding to a disc centered in the segment. Finally, an along-tract profile was generated for each tract.

Experimental design and statistical analysis

We ran the protocol on the dataset of 113 participants (Figure 1, Stage 3), successfully reconstructing the 39 MD-PFC tracts. To examine the extent to which this protocol can reliably reconstruct the tracts and then generate tract metrics, we tested the reproducibility of the protocol across two scanning sessions, on a subset of 24 participants, who returned for a second acquisition session within a mean temporal interval of 15 days. We examined how consistently our protocol reconstructed the tracts and tractometry at these two different time points.

To measure the test-retest reproducibility, we quantitatively analyzed the similarity of two tracts at both microstructural and macrostructural levels. At the *microstructural level*, to evaluate

reproducibility in tractometry generation, we performed pairwise Pearson correlations on tract profiles across test and retest sessions using scipy (Virtanen et al., 2020). For simplicity, we only show the correlations for FA values, as this is the most widely used metric in the literature. Other diffusion summary statistics showed similar patterns. At the *macrostructural level*, we calculated the Dice overlap index to evaluate the volume-based overlap between test and retest sessions. We also measured the streamline density correlation and the average distance between streamlines from two tracts, which showed similar patterns to the Dice overlap index, thus are not reported here. The Dice overlap index was computed using the package scilpy (see details in (Schilling et al., 2021) and https://github.com/scilus/scilpy). Distributions, group means and standard deviations are reported for both Pearson correlation and Dice overlap index results.

Code and data accessibility

The protocol and parameters to reconstruct and measure the tracts, as well as custom codes for statistical analysis and figure generation are available on github (https://github.com/MengxingLiu/THATRACT2_paper). Raw DWI data used to develop this protocol can be found at https://osf.io/kdch3/.

Results

White-matter tracts linking MD with all 39 PFC areas are detectable with our protocol

We designed a new tractography protocol (see Methods) for the delineation from DWI data of the white-matter tracts connecting MD with each one of the 39 PFC areas identified in the HCP atlas and organized in four PFC group regions (Glasser et al., 2016). In all individuals tested, the protocol detected a sizable bundle of connections extending between the MD and each one of the PFC areas. As an example, the 39 tracts from the left hemisphere traced in a representative individual are illustrated in Figure 2. Because of the large number of cortical areas under investigation, for organizational purposes, we grouped the tractographies into four broad PFC group regions, according to their cortical target areas, following the multiarea “regions” proposed by Glasser et al. (2016) based

both on the contiguous position of the corresponding areas in the frontal lobe surface as well as on shared common properties such as myeloarchitecture, general task-fMRI profiles, and/or functional connectivity. Namely, these four group regions were: (a) tracts linking MD with areas in the dorsolateral group region of the PFC (dPFC), which includes 13 areas: the BA8C (8C); ventral BA8A (8Av); inferior transitional area between BA6 and BA8 (i6-8); superior transitional area between BA6 and BA8 (s6-8); superior frontal language area (SFL); lateral BA8B (8BL); posterior BA9 (9p); anterior BA9 (9a); anterior dorsal BA8 (8Ad); posterior transitional area between BA9 and ventral BA46 (p9-46v); anterior transitional area between BA9 and ventral BA46 (a9-46v); ; BA46 (46); transitional area between BA9 and dorsal BA46 (9-46d); (b) tracts connecting MD with areas in the medial aspect of the PFC (mPFC) group region, which consists of 7 areas: pregenual BA32 (p32); subgenual BA32 (s32); medial BA8B (8BM); medial BA9 (9m); ventral BA10 (10v); rostral BA10 (10r); BA25 (25); (c) tracts connecting MD with areas situated in the orbital surface or in the polar group region of the PFC (OrbPoPFC), which contains 11 areas: sulcal part of BA47 (47s); medial BA47 (47m); anterior rostral BA47 (a47r); lateral BA11 (11l); lateral BA13 (13l); anterior polar portion of BA10 (a10p); posterior polar portion of BA10 (p10p); most polar portion of BA10 (10pp); dorsal BA10 (10d); orbitofrontal complex (OFC); posterior orbitofrontal complex (pOFC); and (d) tracts connecting MD with areas in the inferolateral/opercular prefrontal cortex (IFC) group region, which includes 8 areas: BA44 (44); BA45 (45); posterior junction of the inferior frontal and the precentral sulcus (IFJp); anterior junction of the inferior frontal and the precentral sulcus (IFJa); posterior inferior frontal sulcus (IFSp); anterior inferior frontal sulcus (IFSa); lateral BA47 (47l); posterior rostral BA47 (p47r).

As shown in Figure 2, the fiber bundle connections invariably began at the anterolateral surface of the MD and fanned out in a rostral direction. The global layout of the MD-PFC pathways had a marked “bouquet-like” appearance: all fiber bundles started in MD and extended as a compact “stem” along the anterior limb of the internal capsule, following roughly parallel trajectories. Then, as the trajectories reached the subcortical white matter of the frontal lobe, they fanned out in different directions, each towards its target PFC cortical area. Along this general pathway, the position of each trajectory varied in systematic fashion depending on the location of the target PFC cortical area.

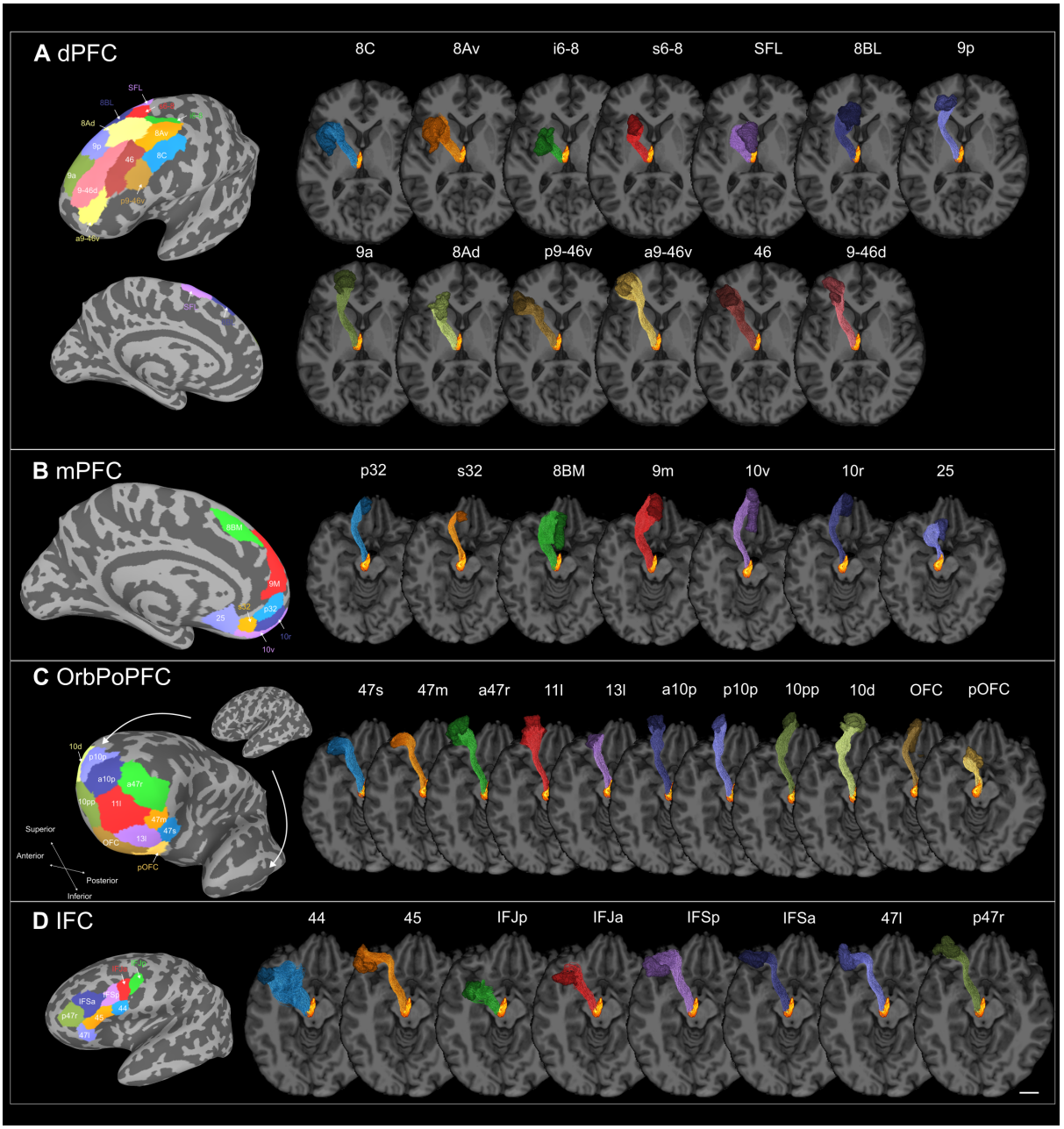

Figure 2. The 39 tracts, shown here in the left hemisphere, are categorized into four broad separate group regions according to their terminating areas in the PFC (Glasser et al., 2016). (**A**) tracts connected to 13 areas within dorsal PFC (dPFC); (**B**) tracts connected to 7 areas within medial PFC (mPFC); (**C**) tracts connected to 11 areas within orbital PFC and frontal pole (OrbPoPFC); (**D**) tracts connected to 8 areas within inferior frontal cortex (IFC). All tracts correspond to the same representative individual. The calibration bar at the bottom right represents 2 cm.

Tractography reveals the fine-grain anatomy of the human MD-PFC pathways

To investigate the anatomical accuracy of tractographies generated with our protocol, we examined them as streamlines in serial two-dimensional (2D) sections. This visualization provides higher anatomical resolution not appreciated in three-dimensional (3D) visualizations, and it is readily comparable to connection-labeling data reported in NHPs and other mammals.

The quality and resolution of these streamlines offered an unprecedented level of anatomical detail about aspects of the layout of the human MD-PFC white-matter tracts. For example, the tract streamlines were clearly visible not only in the cerebral white matter, as is usual in tractographic studies of long-distance pathways, but could also be followed deep into the gray matter of the thalamus, until disappearing within the MD nucleus itself (Figure 3B-E).

First, we examined in 2D sections the differences between the streamlines linking MD to four areas belonging each to one of the large PFC group regions described above (Glasser et al. 2016). Figure 3 shows the comparison between the tractographies from MD to i6-8 (a transitional PFC area bordering visuomotor areas of the dorsal premotor cortex that corresponds to the dPFC group region in Figure 2), to iFSP (a language-associated area in the lower lip of the inferior frontal sulcus that corresponds to the IFC group region in Figure 2), to p32 (located in the anterior area of the cingulate gyrus and involved in emotional expression, attention allocation, and mood regulation; and that corresponds to the mPFC group region in Figure 2) and OFC (an area encompassing part of cytoarchitectonic areas 11, 13 and 14 and functionally related to affective and motivational behavior, and that corresponds to the OrbPoPFC group region in Figure 2). This analysis revealed that the streamlines for each one of these four areas follow separate trajectories in the internal capsule and cortical white matter, and remain distinct as they propagate throughout the thalamus gray matter into MD. As can be appreciated in Figure 3B-E, the streamlines from i6-8 (in purple-pink), terminate only in a lateral portion of MD, while those from IFSp (in yellow) terminate in the central and dorsal domain of MD. The streamlines from p32 (in blue) target a different, more ventral and medial portion of MD. Finally, the streamlines from OFC (in green), terminate even more medially in MD, and some of them reach the small midline nuclei (Paraventricular, Central Medial) medially adjacent to MD.

The analysis also reveals a small zone of overlap between the p32 and OFC streamlines (cyan voxels) both in the internal capsule (Figure 3A) and within MD (Figure 3B-E).

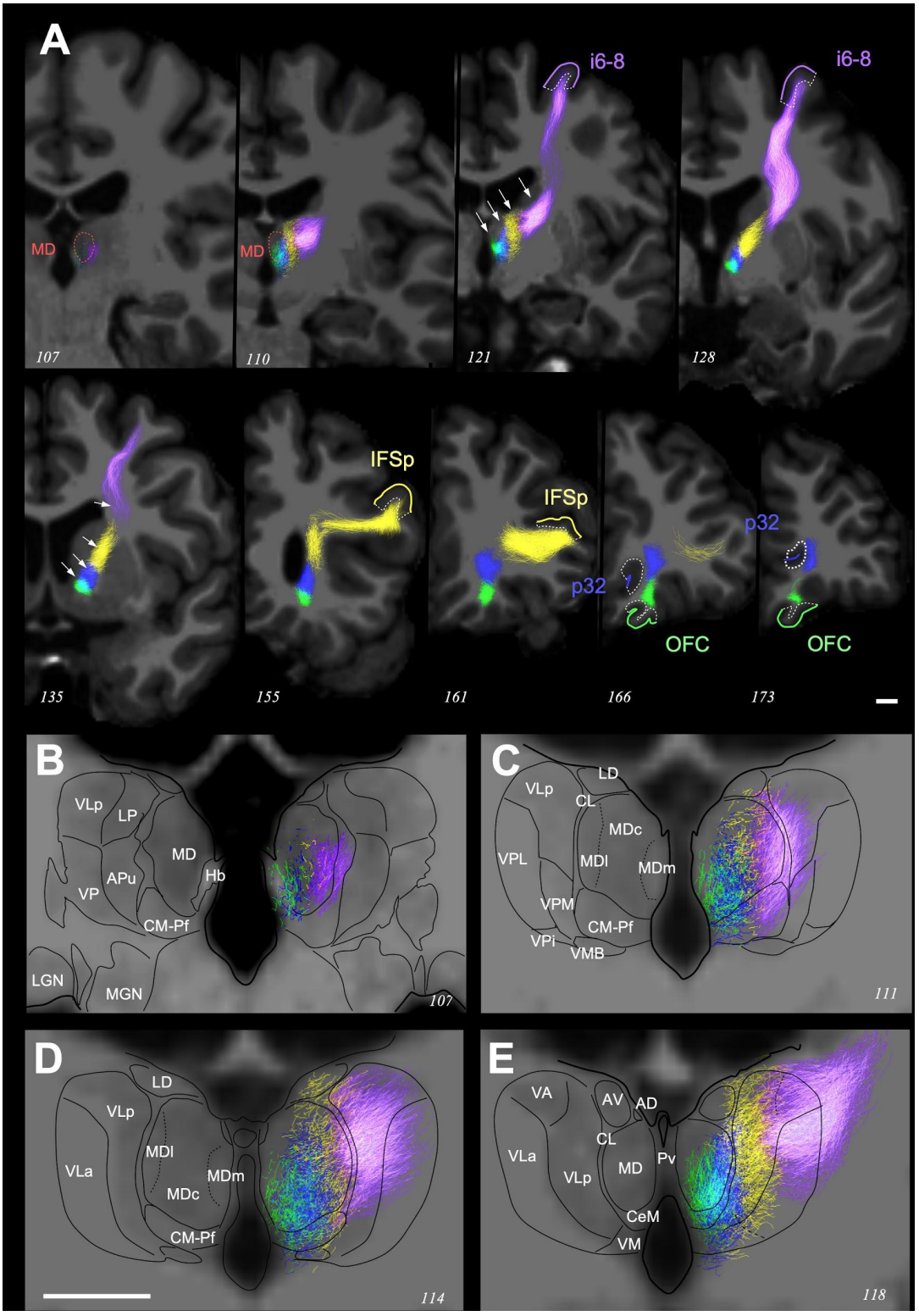

Figure 3. Intra- and extra-thalamic paths of the tracts linking MD with four PFC areas, belonging to separate PFC group regions (Glasser et al., 2016). (**A**) Streamline visualizations of the tractographies between MD (dashed red line contour) and the inferior transitional area between BA6 and BA8 (i6-8, purple), the posterior inferior frontal sulcus (IFSp, part of BA44, yellow), posterior BA32 (p32, blue)

and orbitofrontal complex (OFC, part of BA11, BA13 and BA14, green). The part of the cortex corresponding to each seed area is delineated, and its pial surface is highlighted in color. Each tract is coded in the corresponding color; white indicates coregistration of all four streamlines in the same voxel. Note that the four tracts (arrows) remain distinct all the way from MD to the cortex, with minimal or no overlap (mixed colors) between them. Tractographies are shown on serial 1mm-thick frontal slices. Occipito-frontal distance (in mm) is indicated by the number under each section. In this individual the anterior and posterior commissures were located at levels 132 and 105, respectively. The white line at the bottom right of the panel represents 1 cm. (**B-E**) Coronal sections of both thalami are illustrated at higher magnification. For reference, nuclei delineations based on Hirai & Jones (1989) made on the T1 images are superimposed. Note that each of the four tracts can be followed separately (with minimal or no color blending) into specific subdomains within MD. Calibration bar A-E = 1 cm. Abbreviations: AD, anterodorsal; APu, anterior pulvinar; AV, anteroventral; CeM, central medial; CL, central lateral; CM, centromedian; Hb, habenula; LD, laterodorsal; LGN, lateral geniculate nucleus; LP, lateral posterior; MD, mediodorsal; MDc, mediodorsal central; MDl, mediodorsal lateral; MDm, mediodorsal medial; MGN, medial geniculate nucleus; Pf, parafascicular; Pv, paraventral; VA, ventral anterior; VLa, ventral lateral anterior; VLp, ventral lateral posterior; VM, ventromedial; VMB, ventral medial basal; VP, ventral posterior; VPi, ventral posterior inferior; VPL, ventral posterolateral; VPM, ventral posterior medial.

Next, we applied the 2D analysis to the streamlines linking MD with areas that were part of the same broad anatomo-functional group region (Glasser et al., 2016). First, we compared four large areas in the dPFC group (see Figure 2). Namely, the areas compared were 9p, 9a, 9-46d, a9-46v (Figure 4A). These high-level multimodal areas encompass a large part of the middle frontal gyrus. These areas are richly interconnected with each other and with other parietal and temporal high-level areas (Petrides and Pandya, 1984; Maguire et al., 1999). They are key nodes for networks involved in cognitive functions such as sustaining attention, detecting familiarity, planning, decision making and working memory (Petrides et al., 2012; Glasser et al., 2016). In striking contrast with the areas compared in Figure 3, the four tracts in Figure 4 started from the same central and lateral portions of MD (Fig. 4C-F) and remained strictly overlapped as they exited the thalamus as well as along their path in the internal capsule, all the way into the pallial white matter. The overlap is so strict that most voxels display complete coincidence of the four streamlines in the same voxel (shown as white in Figure 4). In the subcortical white matter, however, the four tracts diverged abruptly, as indicated by the appearance of single-color trajectories that reached the four target areas (Fig. 4A). Most streamlines stopped at the edge of the cortical gray matter, in agreement with the known anatomy of myelinated thalamocortical and corticothalamic tracts (Salami et al., 2003). However, at the crown of some gyri, some streamlines propagated radially into the cortex, up to the cortical middle layers,

consistent with the morphology and abundance of intracortical radial bundles of myelinated axons in the gyral portions of some areas (Figure 4B; Nieuwenhuys, 2013).

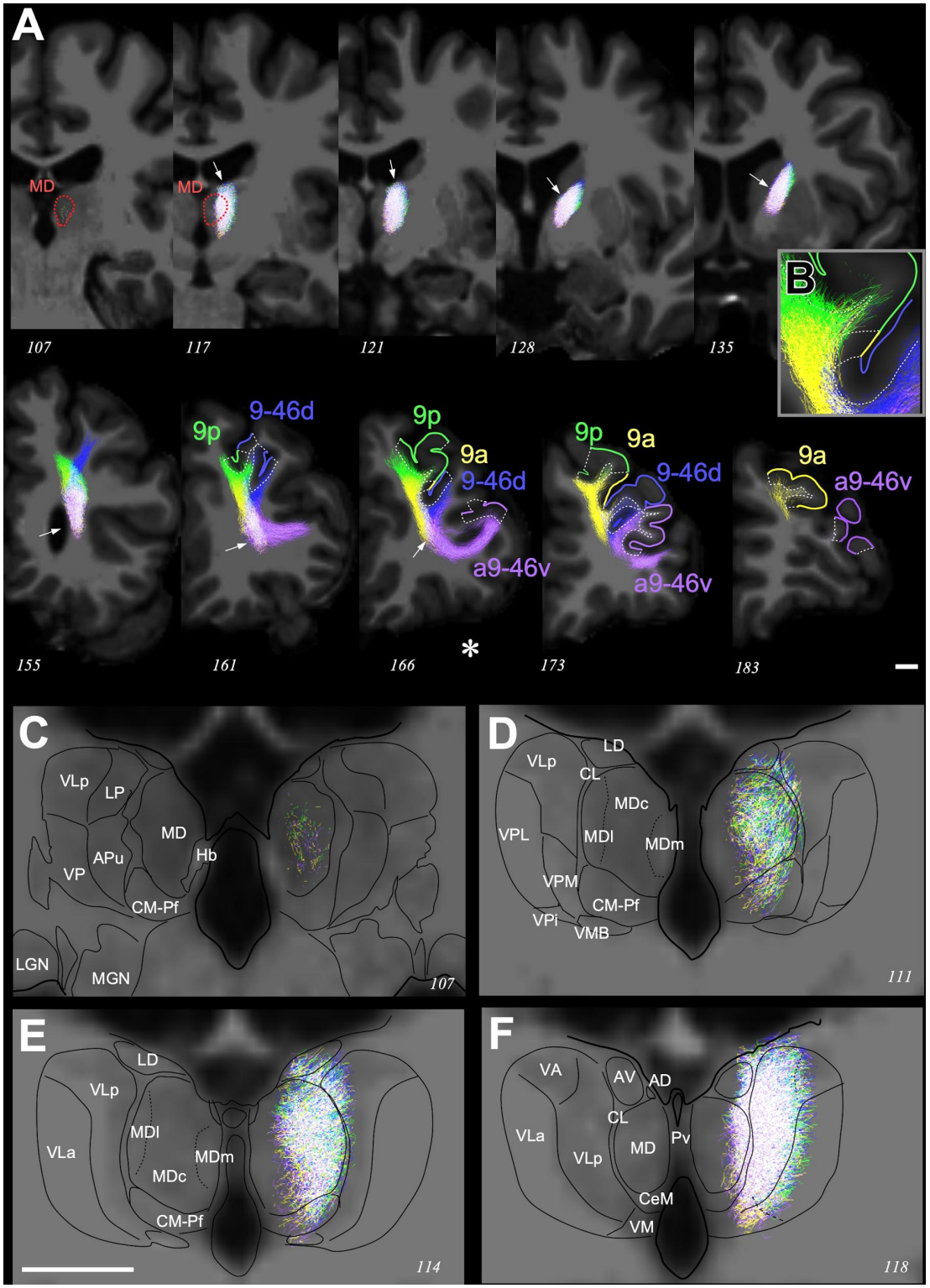

Figure 4. Intra- and extra-thalamic paths of the tracts connecting MD with four cortical areas belonging to the same dPFC group region. (**A**) Streamline visualizations of the tractographies between MD (red line contour) and the inferior transitional area between areas BA9 anterior (9a, yellow); BA9 posterior (9p, green); transitional area between BA9 and dorsal BA46 (9-46d, blue); anterior

transitional area between BA9 and ventral BA46 (a9-46v, purple). The part of the cortex corresponding to each seed area is delineated, and its pial surface is highlighted in color. Each tract is coded in the corresponding color; white indicates coregistration of all four streamlines in the same voxel. Note that the four tracts remain strictly overlapped (arrow) from their origin in MD and in the internal capsule, all the way into the pallial white matter. There, the four tracts split abruptly to follow independent trajectories towards their target areas. The asterisk indicates the coronal slice from which the magnified image shown in panel B was taken. (**B**) Magnified visualization of a coronal slice showing the streamlines reaching cortical areas 9p, 9a and 9-46d. (**C-F**) Coronal sections of both thalami at higher magnification. Tractographies were obtained from the same individual shown in Figure 2. Note that each of the four tracts remain coregistered extensively in the same voxels as they traverse the gray matter of the thalamus and enter MD. Calibration bar A-F = 1 cm. Graphic conventions and abbreviations as in Figure 3.

Figure 5 shows the same analysis conducted for the streamlines from four cortical areas within the mPFC group region (see Figure 2): 10r, 10v, s32 and 25. These ventral and medial PFC areas include a considerable portion of the medial frontal gyrus and are relatively heterogeneous group of areas. Connection tracing studies in macaques indicate that the equivalent areas are richly connected with other ipsi and contralateral PFC areas, as well as with limbic areas across the brain, both isocortical (cingulate, retrosplenial, temporopolar) and non-isocortical (parahippocampal and hippocampus, Porrino et al., 1981; Cavada et al. 2000). Overall, the mPFC areas are involved in processing recent and remote memories, memory consolidation, and adaptive decision making; leading to the suggestion that mPFC regions process the current context and events, and predict the most adaptive response based on past experience (Euston et al., 2012). In contrast with the dPFC areas, the tracts linking MD with these four mPFC areas show a relatively small degree of coregistration to the same voxels (white color), largely limited to the intrathalamic part of the path. The streamlines separate as they advance along the ventral part of the anterior limb of the internal capsule. The streamlines to area 25 (violet in Figure 5) arise from the most medial part of MD as well as from the adjacent midline nuclei (Paraventricular, Central Medial) in the ventricular wall and diverge rapidly from the other three tractographies to terminate in their target area (Figure 5A, C-F). The streamlines to area 10v, which is transitional with the frontopolar cortex, also show limited overlap, as they arise from a relatively central and ventral portion of MD and occupy a relatively central portion of the anterior limb of the internal capsule, resembling in this regard the projections of other frontopolar areas (Figure 5A, B).

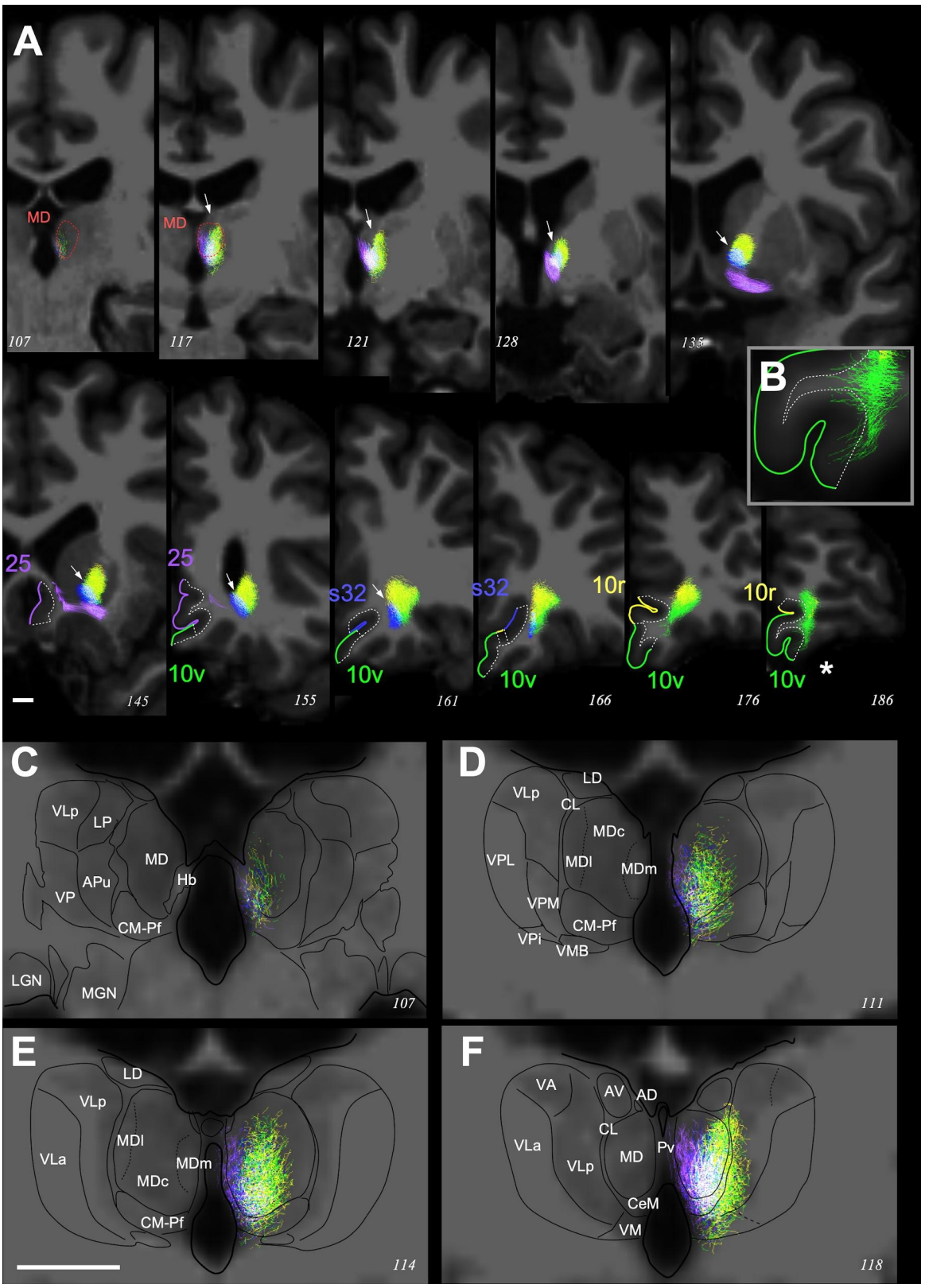

Figure 5. Intra- and extra-thalamic paths of the tracts connecting MD with four cortical areas belonging to the mPFC group region. (**A**) Streamline visualizations of the tractographies between MD (red line contour) and area 10r (yellow); area 10v (green); area s32 (blue); area 25 (purple). The part of the cortex corresponding to each seed area is delineated, and its pial surface is highlighted in color. Each tract is coded in the corresponding color; white indicates coregistration of all four streamlines in the same voxel. Note that the four tracts remain partially corregistered (shown in white and indicated

by an arrow) only near their origin in medial MD. The asterisk indicates the coronal slice from which the magnified image shown in panel B was taken. (**B**) Magnified visualization of a coronal slice showing the streamlines reaching cortical area 10v. (**C-F**) Coronal sections of both thalami at higher magnification. Tractographies were obtained from the same individual shown in Figure 2. Calibration bar A-F = 1 cm. Graphic conventions and abbreviations as in Figure 3.

The analysis for areas within the OrbPoPFC group region (see Figure 2) is shown in Figure 6, which includes the streamlines from 11l, 13l, p10p, and a10p. These PFC areas are located in the orbital and polar portions of the frontal cortex. Studies in macaques indicate that the equivalent frontal areas are richly interconnected with the contralateral and ipsilateral PFC areas as well with limbic areas in the cingulate and temporal cortices (Porrino et al., 1981; Cavada et al, 2000). The medial rostral BA10 has been associated with attending to one's own emotions and mental states (Gilbert et al., 2006a) and switching attention between current sensory input and internally generated thought processes (Gilbert et al., 2006b). Orbital areas 11 and 13 are typically found to be involved in updating and storing outcome-specific information and decision making (Rudebeck and Rich, 2018). The tracts from MD to these four areas (Figure 6A-F) arose from the central and anterior portion of MD and remained substantially overlapped along their trajectories in the anterior limb of the internal capsule, especially in the case of the streamlines targeting areas 11l and a10p, which only separated near their target areas (Figure 6A, B). The streamlines to area 13l showed the least coregistration; they originated mostly in medial MD and occupied a more ventral position in the internal capsule than the other three areas (Figure 6C-F).

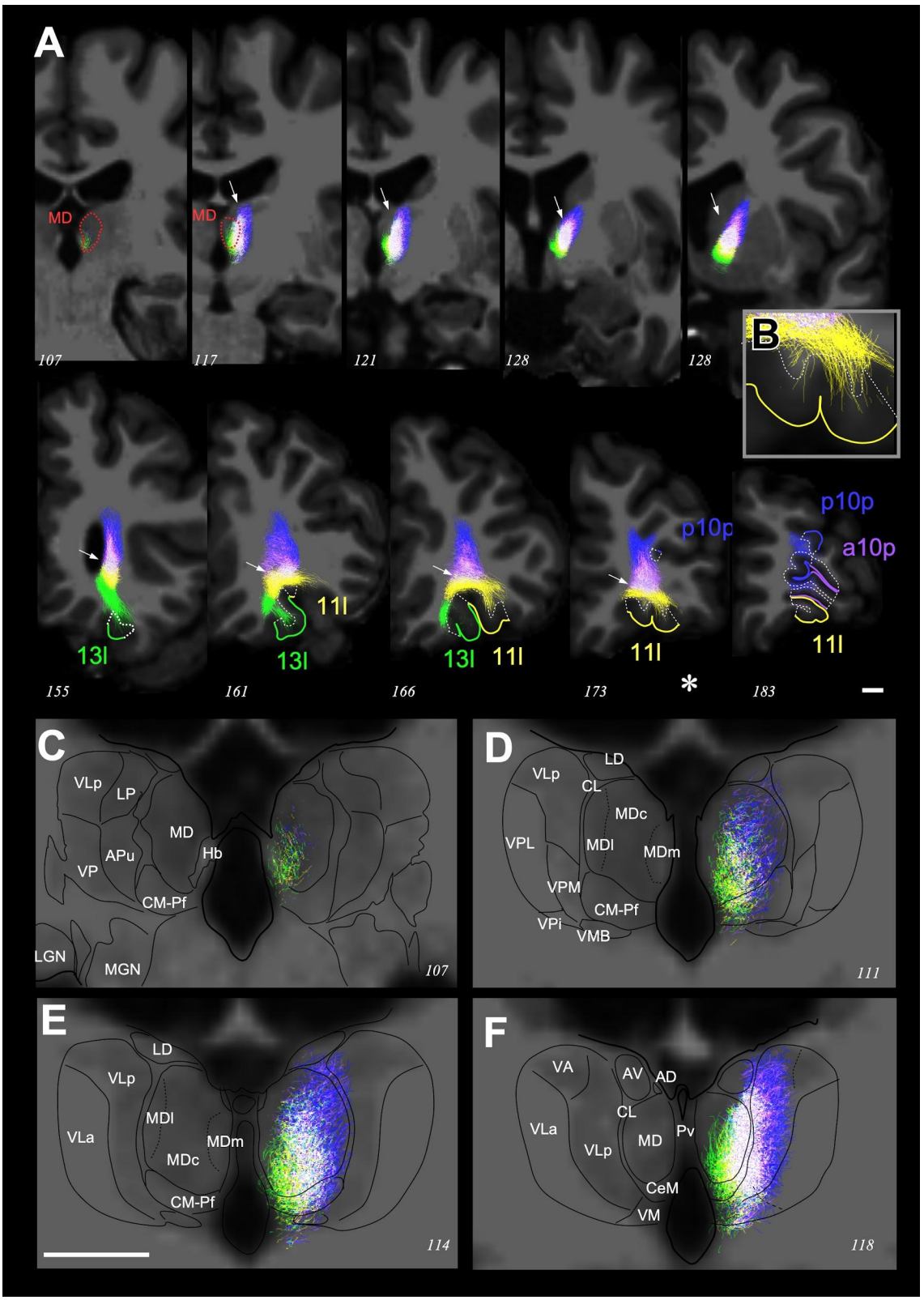

Figure 6. Intra- and extra-thalamic paths of the tracts connecting MD with four cortical areas in the OrbPoPFC group region. (**A**) Streamline visualizations of the tractographies between MD (red line contour) and area 11l (yellow); area 13l (green); area p10p (blue); area a10p (purple). The part of the cortex corresponding to each seed area is delineated, and its pial surface is highlighted in color. Each tract is coded in the corresponding color; white indicates coregistration of all four streamlines in the same voxel. Note that the four tracts remain partially coregistered to the same voxels (shown in white and indicated by an arrow) as they traverse the gray matter of the thalamus and the anterior limb of

the internal capsule. The asterisk indicates the coronal slice from which the magnified image shown in panel B was taken. (**B**) Magnified visualization of a coronal slice showing some streamlines propagating radially into the middle layers of cortical area 11l. (**C-F**) Coronal sections of both thalami at higher magnification. Tractographies were obtained from the same individual shown in Figure 2. Calibration bar A-F = 1 cm. Graphic conventions and abbreviations as in Figure 3.

Finally, we analyzed the streamline tractographies linking MD with four areas from the IFC group region in serial 2D sections (see Figure 2). The areas examined in this case were 45, 47l, IFSa and IFSp (Figure 7). These high-level IFC areas (or their equivalent territories in macaques) share functional network affiliations as they are richly interconnected with each other and with other temporal and parietal areas (Cavada et al., 2000; Petrides and Pandya, 2009; Frey et al., 2014). In humans, they are key nodes for networks involved in language processing, speech production, sound-to-meaning comprehension and controlled retrieval and selection of information (Petrides and Pandya, 2009). Similar to the dPFC streamlines (Figure 4), the tracts from MD to these four areas arose mostly from central portions of the MD (Figure 7C-F). The tracts coregistered extensively to the same voxels in the internal capsule (see white arrows in Figure 7A), but then split in the subcortical white matter. In this case, the tract directed to area 47L, which borders the orbital cortex areas, is the most medially situated and shows less overlap with the rest. In contrast, the streamlines for target areas 45 and IFSp remain overlapped until the immediate vicinity of their target areas in the cortex (Figure 7A). In addition, some streamlines to these areas propagated radially until the cortical gray matter, up to its middle layers (Figure 7B).

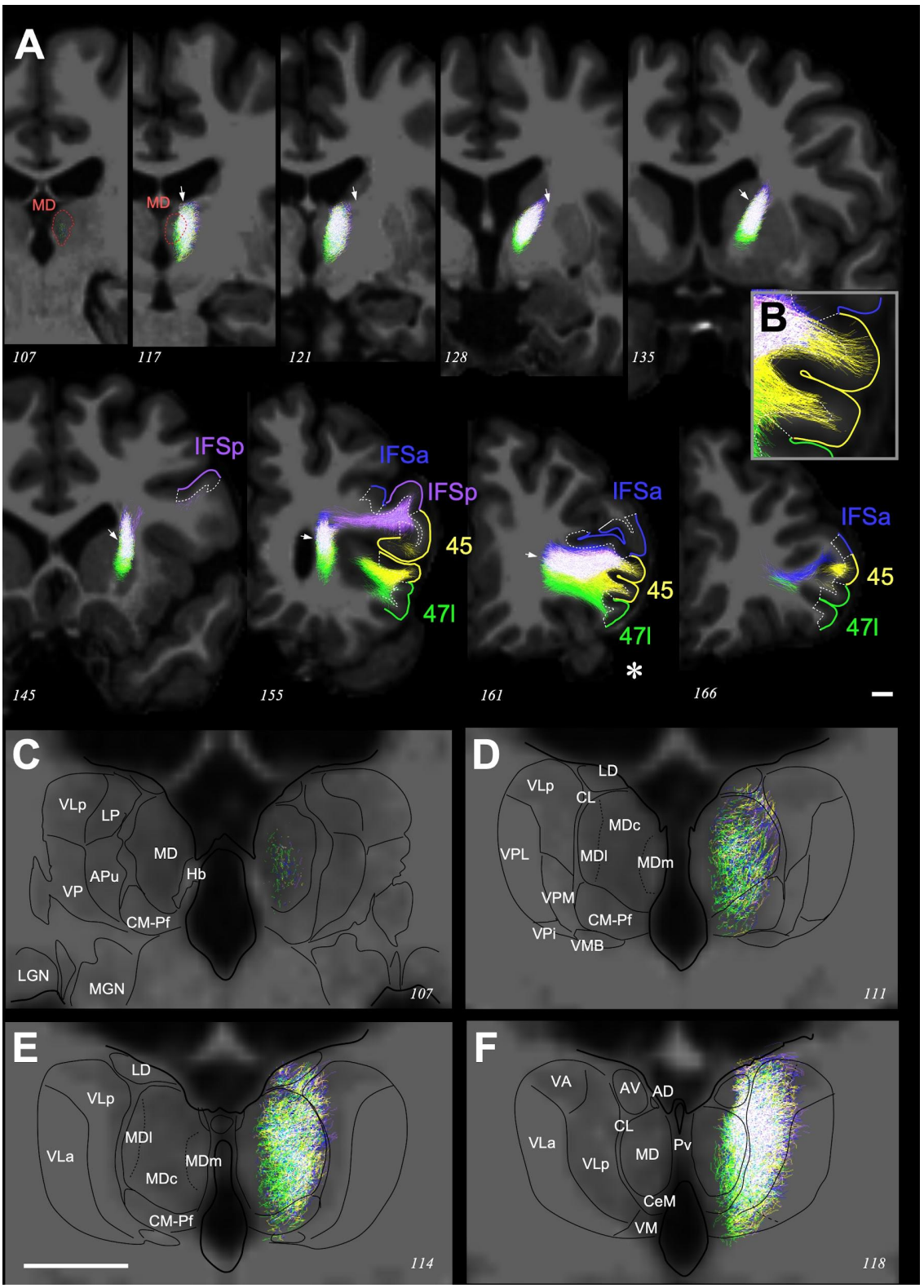

Figure 7. Intra- and extra-thalamic paths of the tracts connecting MD with four cortical areas belonging to the same IFC group region. (**A**) Streamline visualizations of the tractographies between MD (red line contour) and area 45 (yellow); area 47l (green); area IFSa (blue); area IFSp (purple). The part of the cortex corresponding to each seed area is delineated, and its pial surface is highlighted in color. Each tract is coded in the corresponding color; white indicates coregistration of all four streamlines in the same voxel (indicated by an arrow). Note that the tracts coregistered extensively (arrow) from their origin in MD and in the internal capsule, all the way into the subcortical white

matter where they split, with the tract directed to area 47L showing less overlap with the others. The asterisk indicates the coronal slice from which the magnified image shown in panel B was taken. (**B**) Magnified visualization of a coronal slice showing the streamlines radiating into the middle layers of cortical area 45. (**C-F**) Coronal sections of both thalami at higher magnification. Tractographies were obtained from the same individual shown in Figure 2. Calibration bar A-F = 1 cm. Conventions and abbreviations as in Figure 3.

Test-retest reproducibility analyses of the protocol

To examine test-retest reproducibility at both microstructural and macrostructural levels for all the MD-PFC tracts within each of the four PFC group regions we used test-retest data from a subset of 24 participants (Figures 8-11; see also https://osf.io/kdch3/ for tables with group means and standard deviations for test-retest microstructural and macrostructural results). At the microstructural level, the tracts within the dPFC group area showed high test-retest reproducibility for the FA correlation profile (see Fig. 8B for FA test-retest values along the length of four pathways), with a group mean range of 0.98-0.99 (Fig. 8C1). At the macrostructural level, these tracts demonstrated good test-reproducibility with the Dice index showing a group mean ranging from 0.86 to 0.93 (Fig. 8C2).

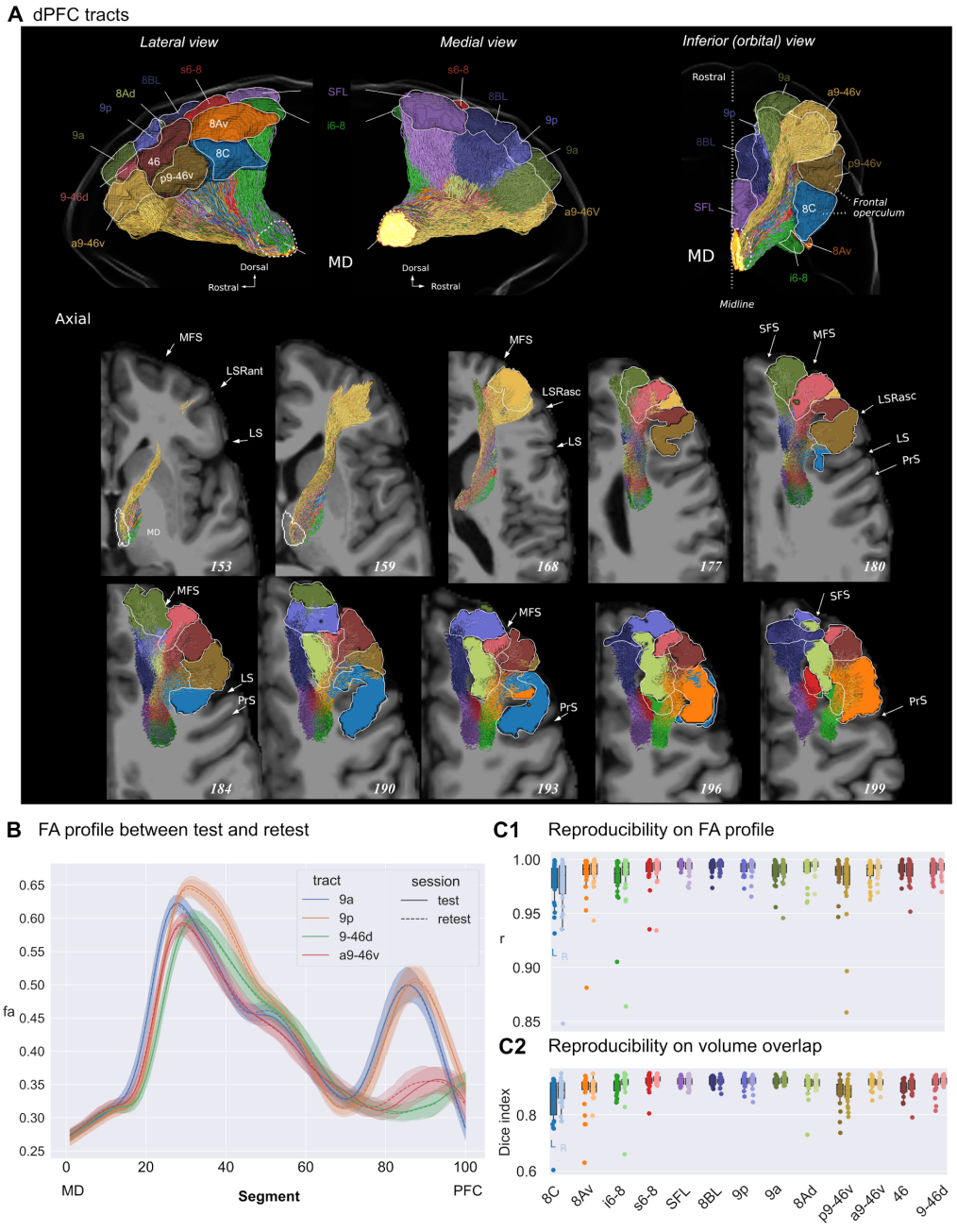

Figure 8. Test-retest reproducibility of tracts connecting MD with areas within the dPFC group region. (**A**) The volume and slice views of all the dPFC reconstructed tracts in a representative participant. Color scheme is the same as used in C panel. (**B**) FA values between test and retest along the MD-PFC pathway length of four selected tracts. Shaded areas represent 95% confidence intervals. (**C**) Test-retest reproducibility: **C1**) strip plots showing the distribution of FA correlation coefficients between test and retest for each tract and each participant (lighter color columns represent the left hemisphere; darker color columns represent the right hemisphere). Each dot represents the correlation coefficient for one participant; Box-and-whisker plots are overlaid on top to show the quartiles of the distribution. **C2**) The Dice overlap between test and retest for each tract and each subject. Abbreviations: LS, lateral sulcus; LSRant, lateral sulcus anterior ramus; LSRasc, lateral sulcus ascendens ramus; MFS, middle frontal sulcus; PrS, principal sulcus; SFS, superior frontal sulcus.

Similarly, the mPFC group tracts also showed high test-retest reproducibility with tracts showing a group mean range of 0.71-0.99 at the microstructural level (see Fig. 9B & 9C1 for FA and FA correlation profiles, respectively) and a group mean range of 0.78-0.91 at the macrostructural level (see Fig. 9C1 for Dice values), with a few exceptions showing a moderate reproducibility: the left BA25 tract with a FA correlation profile of 0.64 and a Dice overlap of 0.58; and the right BA25 and s32 tracts with Dice overlap values of 0.67 and 0.68, respectively (see Fig. 9C1 and C2).

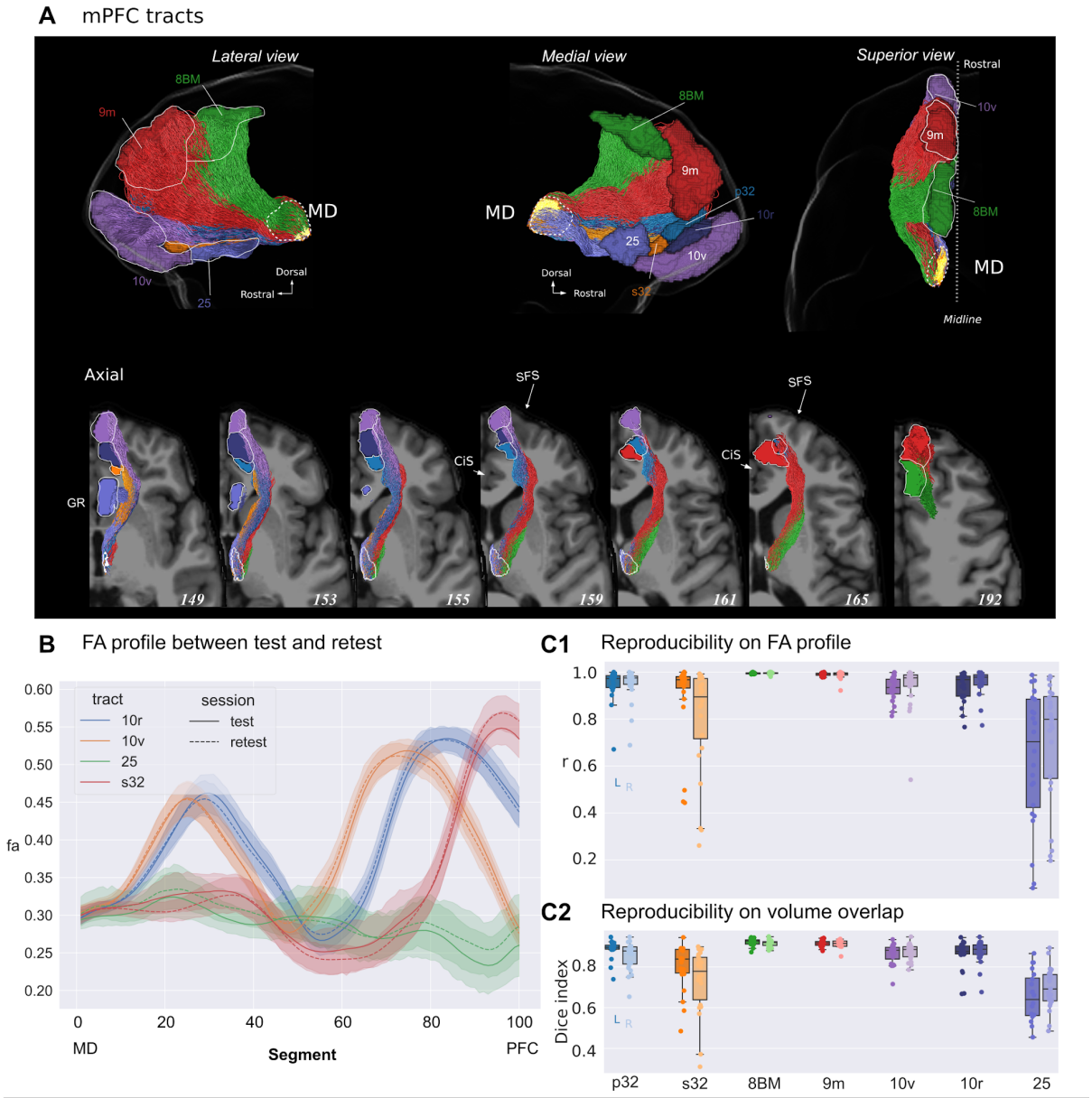

Figure 9. Test-retest reproducibility of tracts connecting MD with areas within the mPFC group region. (**A**) The volume and slice views of all the mPFC reconstructed tracts in a representative participant. Color scheme is the same as used in C panel. (**B**) FA values between test and retest along the MD-PFC pathway length of four selected tracts. Shaded areas represent 95% confidence intervals. (**C**) Test-retest reproducibility: **C1**) strip plots showing the distribution of FA correlation coefficients

between test and retest for each tract and each participant (lighter color columns represent the left hemisphere; darker color columns represent the right hemisphere). Each dot represents the correlation coefficient for one participant; Box-and-whisker plots are overlaid on top to show the quartiles of the distribution. **C2**) The Dice overlap between test and retest for each tract and each subject. Abbreviations: CiS, cingulate sulcus; GR, gyrus rectus; SFS, superior frontal sulcus.

As for the tracts reaching OrbPoPFC areas, the FA correlation profiles were above 0.8 except for the right pOFC tract, which has a group mean of 0.72 (Fig. 10C1; see also Fig. 10B for FA test-retest values along the length of four pathways). At the macrostructural level, the tracts within this group area showed a group mean range of 0.78-0.91, with the exception of bilateral pOFC tracts showing relatively more variance with Dice overlap values at 0.66 and 0.72 for the left and right hemisphere respectively (Fig. 10C2).

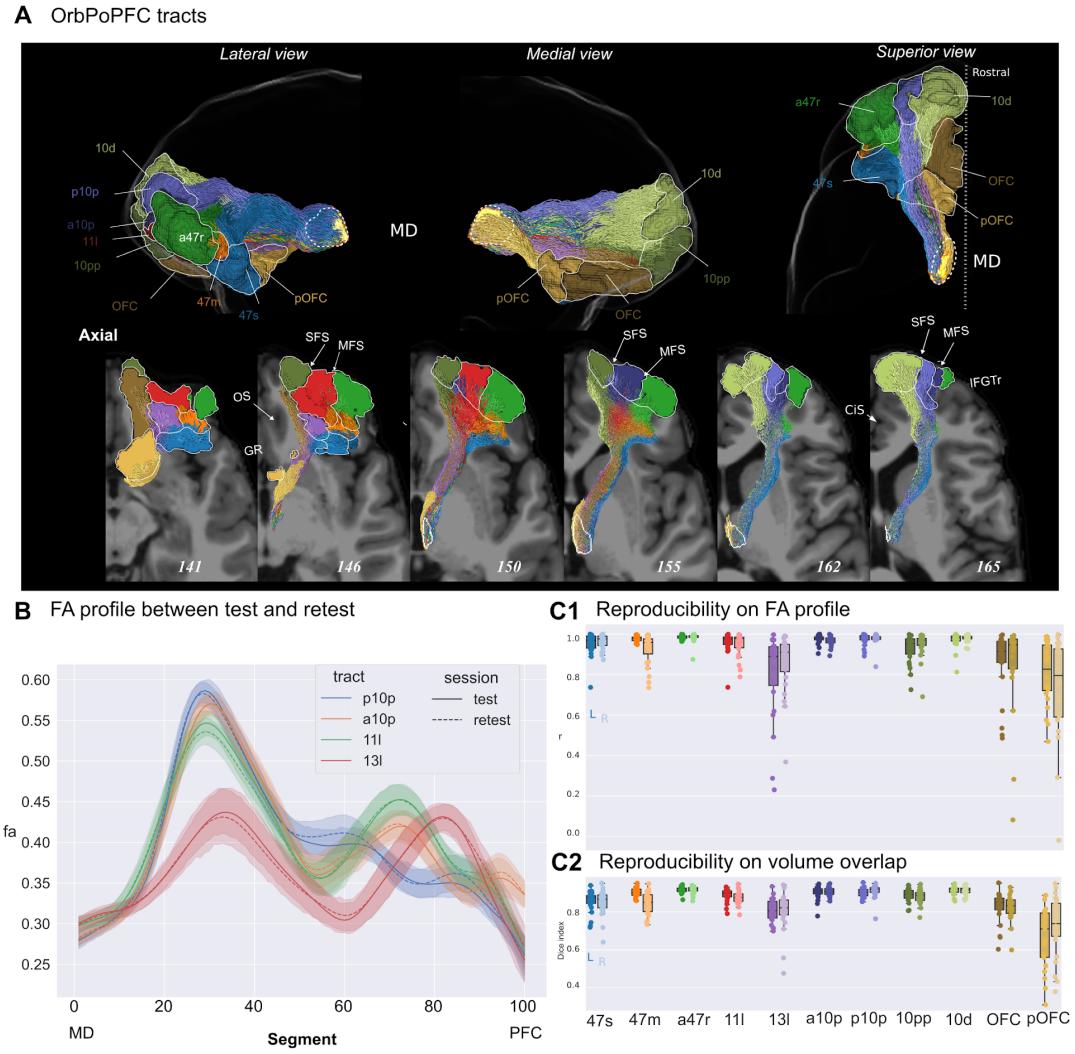

Figure 10. Test-retest reproducibility of tracts connecting MD with areas within the OrbPoPFC group region. (**A**) The volume and slice views of all the OrbPoPFC reconstructed tracts in a representative participant. Color scheme is the same as used in C panel. (**B**) FA values between test and retest along

the MD-PFC pathway length of four selected tracts. Shaded areas represent 95% confidence intervals. (**C**) Test-retest reproducibility: **C1**) strip plots showing the distribution of FA correlation coefficients between test and retest for each tract and each participant (lighter color columns represent the left hemisphere; darker color columns represent the right hemisphere). Each dot represents the correlation coefficient for one participant; Box-and-whisker plots are overlaid on top to show the quartiles of the distribution. **C2**) The Dice overlap between test and retest for each tract and each subject. Abbreviations: CiS, cingulate sulcus; GR, gyrus rectus; IFGTr, inferior frontal gyrus triangular part; MFS, middle frontal sulcus; OS, olfactory sulcus; SFS, superior frontal sulcus.

Finally, all the tracts connecting MD and areas within the IFC group have high test-retest reproducibility at the microstructural level with a group mean of FA correlation profile above 0.90, except for the left IFJa with a group mean of 0.89 (Fig. 11C1; see also Fig. 11B for FA test-retest values along the length of four MD-IFC pathways). The bilateral IFJa and IFJp showed moderate test-retest reproducibility at the macrostructural level, with the Dice overlap ranging from 0.75 to 0.80. All other tracts have Dice overlaps above 0.8 (Fig. 11C2).

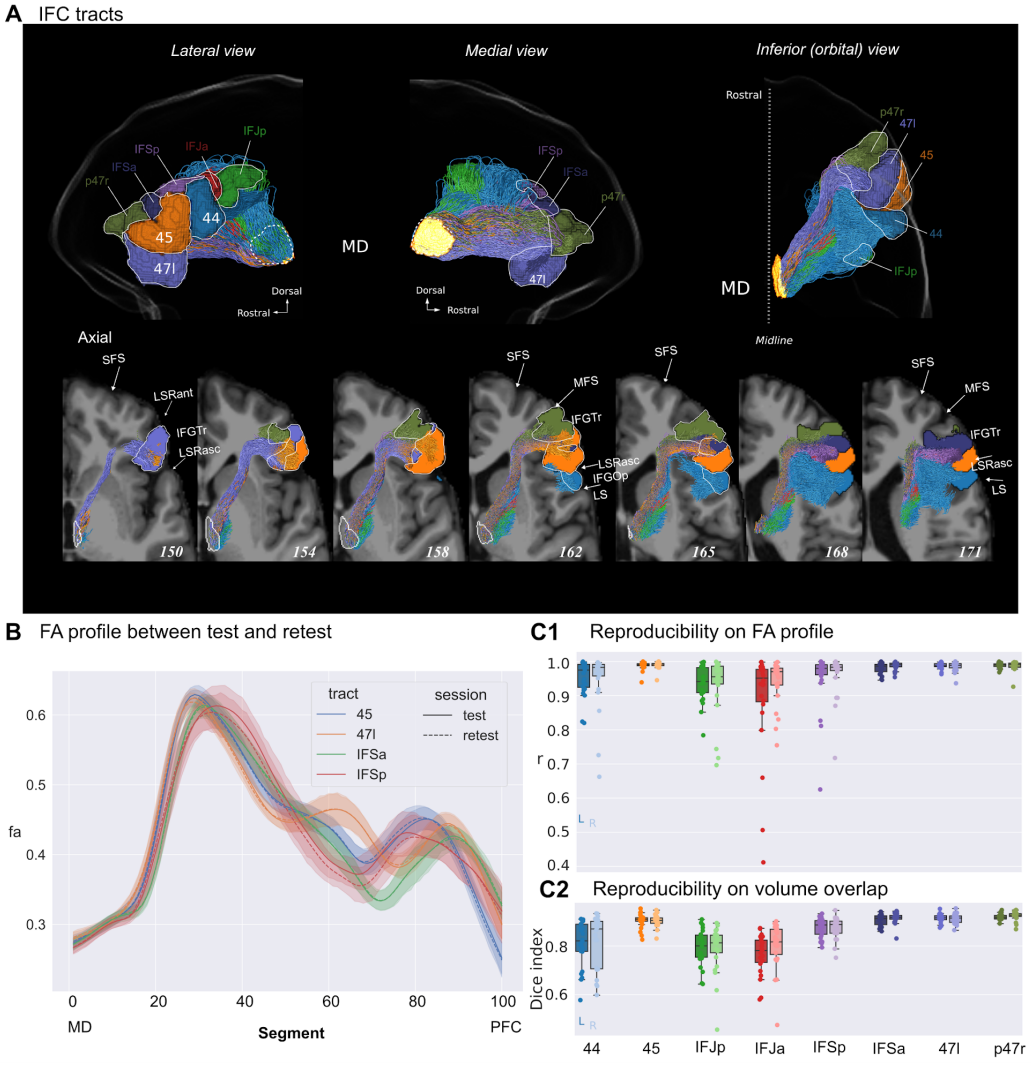

Figure 11. Test-retest reproducibility of tracts connecting MD with areas within the IFC group region. (**A**) The volume and slice views of all the IFC reconstructed tracts in a representative participant. Color scheme is the same as used in C panel. (**B**) FA values between test and retest along the MD-PFC pathway length of four selected tracts. Shaded areas represent 95% confidence intervals. (**C**) Test-retest reproducibility: **C1**) strip plots showing the distribution of FA correlation coefficients between test and retest for each tract and each participant (lighter color columns represent the left hemisphere; darker color columns represent the right hemisphere). Each dot represents the correlation coefficient for one participant; Box-and-whisker plots are overlaid on top to show the quartiles of the distribution. **C2**) The Dice overlap between test and retest for each tract and each subject. Abbreviations: IFGOp, inferior frontal gyrus opercular part; IFGTr, inferior frontal gyrus triangular part; LS, lateral sulcus; LSRant; lateral sulcus anterior ramus; LSRasc, lateral sulcus ascendens ramus; MFS, middle frontal sulcus; SFS, superior frontal sulcus.

Discussion

We present a new tractography reconstruction protocol based on *in vivo* diffusion MRI to measure fiber tracts interconnecting the MD with each of the 39 PFC areas delineated in the HCP atlas (Glasser et al., 2016). The high spatial resolution of the tractographies reveals the anatomical layout of the human MD-PFC pathways with unprecedented detail. Moreover, the protocol shows excellent reproducibility for obtaining the microstructural tractometric properties and good volume-based macrostructural similarity across test and retest sessions.

Neuroanatomical insights provided by the tractographic data

Neuroanatomical information on the thalamocortical and corticothalamic circuits linking the human PFC and MD remains largely an extrapolation from axonal transport connection labeling studies in NHPs and other mammals (Nieuwenhuys et al., 2008). As these highly invasive techniques are not applicable to humans, inferences have remained tentative, given the unique expansion in size and complexity of the human prefrontal and premotor areas (Smaers et al., 2017; Preuss and Wise 2021). Recent advances in MRI-based tractography (Basser et al., 1994; Mori et al., 1999), along with the development of increasingly detailed and accurate voxel-based atlases of the cortex (Glasser et al., 2016) and thalamus (Iglesias et al., 2018), are now opening the possibility of non-invasively examining these pathways in humans. We recently showed that advanced probabilistic DWI methods can trace and measure with high resolution and reliability the axonal tracts linking the main sensorimotor thalamic relay nuclei with their corresponding cortical and cerebellar areas (Liu et al., 2022). The present DWI protocol for non-invasively visualizing, tracing and measuring human

MD-PFC pathways provides key insights into the anatomical organization of these pathways. Below, we discuss the four most novel and relevant insights.

First, the protocol reveals the sub-nuclear organization of MD-PFC connections. Despite the MD seed region including the whole MD, the fiber bundles traced from each PFC area always terminated in a limited portion of the nucleus, leaving most of the seed volume empty. This topography was readily evident because the streamlines propagated deeply into the gray matter of the thalamus, until disappearing within the MD nucleus itself (Figure 3B-E). Moreover, there was an orderly correspondence between the PFC areas and the point of termination of the streamlines within MD. This ordering is most evident when the tractographies of four cortical areas each belonging to a different anatomo-functional PFC group region are directly compared (Figure 3), but it is also detectable by comparing the termination in MD of multiple areas from each PFC group region (Figures 4-7). Unlike the terminal corticothalamic axon arborizations, thalamocortical axons inside the thalamic gray matter are unbranched, thick and heavily myelinated from their origin (Salami et al., 2003) and they travel packed in bundlets (Jones 2007). Thus, the intrathalamic streamlines likely represent mainly thalamocortical MD axons.

Second, the topographic pattern of termination within MD of the streamlines linking this nucleus with the various PFC territories bears a striking resemblance to the topography of thalamocortical (Warren and Akert 1964; Goldman-Rakic and Porrino, 1985; Barbas et al., 1991; Ray and Price, 1993; Inase et al., 1996; Cavada et al., 2000; McFarland and Haber 2002; Erickson and Lewis, 2004; Morel et al., 2005) and corticothalamic (Goldman-Rakic and Porrino, 1985; Preuss and Goldman-Rakic 1987; Siwek and Pandya, 1991; Cavada et al., 2000; McFarland and Haber 2002; Schmahmann et al., 2009) connections described with different connection tracing methods in macaques (Figure 12). In both humans and macaques, the medial “magnocellular” portion of the nucleus (Hirai and Jones, 1989) is connected to isocortical and allocortical areas in orbital and ventromedial portions of the PFC. The extensive central “parvocellular” MD division is connected selectively with granular dorsolateral, dorsoventral and polar PFC areas. And the lateral “paralaminar” portion of MD is chiefly connected with frontal oculomotor and premotor areas. Our data indicate that despite the large non-allometric evolutionary increase in the extent of the isocortical areas in humans

compared to macaques (Smaers et al. 2017, Preuss and Wise 2021), the general MD-PFC connections have diverged minimally between the two anthropoid primate lineages.

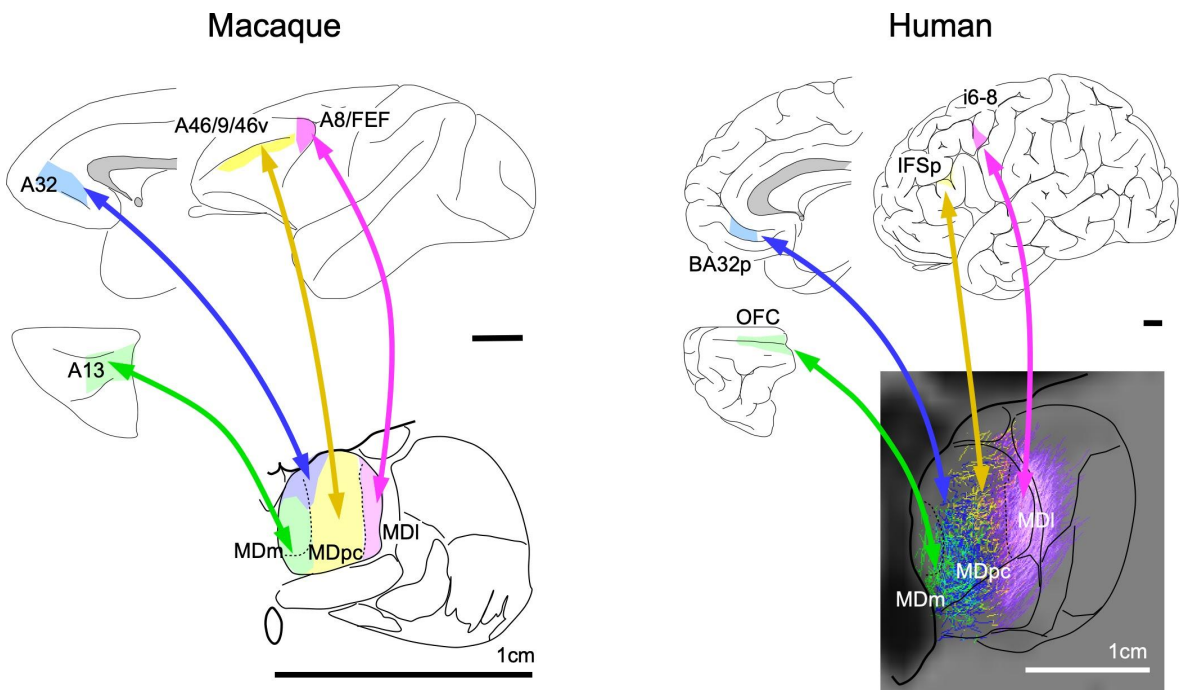

Figure 12. Representation of the MD-PFC connections topologies in macaque (left) and human (right). Calibration bar = 1cm. Abbreviations: MDl, mediodorsal nucleus lateral division; MDm, mediodorsal nucleus magnocellular division; MDpc, mediodorsal nucleus parvocellular division. Macaque cortical areas: A46/9/46v, areas 46, 9 and 46 ventral in the ventral bank of the principal sulcus; A8/FEF, frontal eye fields; A32, area 32, prelimbic cortex; A13, area 13 of the agranular/dysgranular orbital cortex. Macaque connection data based on Warren and Akert, 1964; Goldman-Rakic and Porrino, 1985; Barbas et al., 1991; Ray and Price, 1993; Inase et al., 1996; Cavada et al., 2000; McFarland and Haber, 2002; Erickson and Lewis, 2004; and Morel et al., 2005.

The topography of human MD-PFC connections also bears some resemblance to those between MD and frontal areas of rodents (Groenewegen, 1988; Matyas et al., 2014; Alcaraz et al., 2016; Kuramoto et al., 2017). However, only the connections of the agranular frontal/anterior cingulate areas 25 and 32 with the medial MD seem to be directly comparable, as the equivalence of these cortical areas in rodents and anthropoid primates is relatively well established. For other PFC areas the grounds for comparison are far less clear (for reviews see Carlén, 2017, and Preuss and Wise, 2021).

Third, in contrast with the segregation of streamlines linking MD to areas belonging to different PFC anatomo-functional groups (Figure 3), the streamlines linking MD to areas that belong to the same general anatomo-functional PFC group region originate in roughly the same MD

subregion and often coregister to the same voxels extensively along their path in the internal capsule, before diverging in the subcortical white matter toward their target areas. Coregistration is maximal for areas within the dPFC and IFC groups (Figures 4, 7, 8B, 11B). There is also substantial overlap within the thalamus between streamlines linking the MD with OrbPoPFC areas. However, those going towards orbital area 13l arise more medially and already diverge from the tracts to polar areas p10p and a10p in the internal capsule (Figures 6 and 10B). This observation is consistent with the heterogenous pool of agranular periallocortical and granular isocortical areas in the OrbPoPFC group, and suggests the existence of independent pathways, consistent with the macaque literature (Barbas et al., 1991; Ray and Price 1993). Coregistration is also limited between the streamlines of the mPFC group, which is likewise composed of basal mammalian agranular/dysgranular areas (25 and 32) and granular polar areas selectively expanded in our lineage (10v, 10r, Figure 9B; Preuss and Wise 2021).

Fourth, the tractography data are consistent with the presence of branched thalamocortical axons targeting functionally related PFC areas. This conclusion is based on the strict overlap within the thalamus as well as along the internal capsule between the streamlines directed to two or more functionally related areas. Observations from NHPs studies using double retrograde labeling methods reported the existence of MD neurons innervating more than one PFC area (Goldman-Rakic and Porrino, 1985; Ray and Price, 1993). Such neurons were reportedly a small percentage of all labeled MD cells, but this may be an underestimation, given the high false-negative in double retrograde labeling methods (Schofield et al., 2007). Interestingly, these double-labeled MD cells were found following tracer injections in areas of the same PFC sector, but not when the injections were made in areas belonging to different functional sectors. This evidence in NHPs aligns with single-cell axon reconstruction studies in rats showing that the MD axons branch to innervate more than one frontal area (Kuramoto et al., 2017). It is believed that branched axons simultaneously innervating functionally related areas may favor coupled activity (Casas-Torremocha et al., 2019) and regulate functional connectivity within and among them (Halassa and Kastner, 2017).

Reproducibility of the imaging protocol

Reproducibility is crucial in tractography pipelines. In the current study, after obtaining 39 left and 39 right MD-PFC tracts, we estimated their microstructural and macrostructural properties at test and retest sessions. Test-retest reproducibility is an important indicator to assess reliability for longitudinal studies and potential clinical applications. Our protocol has proved to have good-to-excellent test-retest reproducibility on both microstructural and macrostructural levels. However, specific tracts showed moderate reproducibility on both FA correlation profile and Dice, for example, the ones reaching mPFC, which is close to the midline. This could be due to the relatively low signal-to-noise ratio (SNR) typically obtained in the midline with MRI data (Bellgowan et al., 2006). A previous study showed that low SNR could affect the inter-session reproducibility of the diffusion tensors, such as FA (Farrell et al., 2007). Further systematic examination is needed to confirm this interpretation of the effect of SNR in midline areas on rest-retest reproducibility. We also observed that the Dice overlap was more sensitive to differences between test and retest than the FA correlation profiles. This is because the Dice index is measuring the overlap of the voxels that the digitalized fiber streamlines are trespassing, whereas the FA correlation profile is summarizing the diffusion property of every fiber streamline. Therefore, small differences in streamline locations do not have a large effect on the summarized FA correlation profile, but could affect the Dice overlap, in line with previous reproducibility results on major tracts in the human brain (Zhang et al., 2019). Overall, our protocol was able to reconstruct the 39 left-right pairs of tracts in all 113 participants, with consistent tract volumes and microstructural profiles across test and retest in a subset of 24 participants. This is an important achievement considering the number of tracts we reconstructed and their novelty in the field. Also, an accurate and reproducible quantification of the MD-PFC anatomical connectivity distributions is key to non-invasively investigate the functions carried out by these circuits.

Nevertheless, several limitations of the protocol and potential future directions must be considered. First, the thalamic seed used to reconstruct the MD-PFC tracts is the combination of the lateral and medial MD. Due to the current resolution of MRI, it is challenging to track streamlines from two subnuclei of the MD separately, especially the lateral MD. Future work should examine the

subnuclei-specific white-matter tracts with PFC with better MRI imaging techniques and tractography algorithms. Second, different DWI acquisition sequences can result in different tract profiles. Thus, future work is needed to examine to what extent the tractography test-retest reproducibility is maintained with the use of different DWI MRI protocols, the magnetic field strength of MRI scanner, number of distinct b-values, angular resolution, etcetera. Third, we showed that the current protocol can reconstruct white-matter tracts with data from healthy adults and demonstrated great reproducibility. In the future it would be relevant to test how the results can be generalized to clinical or special populations. The containerization character of the protocol allows testing of other relevant aspects in future studies with minimal configuration requirements.

Finally, it is also relevant to note that the present work focused on the MD-PFC connections, but MD connections extend to areas outside the PFC, such as those in the anterior cingulate and premotor cortices (Giguere and Goldman-Rakic 1988; Morel et al. 2005). Likewise, there are other thalamic nuclei that are heavily connected with some or all PFC areas. These include the medial pulvinar, the anteroventral, and magnocellular ventral anterior thalamic nuclei (Preuss and Goldman-Rakic 1987; Barbas et al., 1991; Romanski et al., 1997; Cavada et al., 2000; McFarland and Haber 2002; Bohsali et al., 2015). Future studies should characterize these tracts in humans and examine to what extent they converge with/segregate from those described here.

References

Acsady L (2022) Organization of thalamic inputs. In: The thalamus, pp 27–44 Cambridge, UK: Cambridge University Press.

Alcaraz F, Marchand AR, Courtand G, Coutureau E, Wolff M (2016) Parallel inputs from the mediodorsal thalamus to the prefrontal cortex in the rat. Eur J Neurosci 44:1972-1986.

Barbas H, Henion TH, Dermon CR (1991) Diverse thalamic projections to the prefrontal cortex in the rhesus monkey. J Comp Neurol 313:65–94.

Basser PJ, Mattiello J, LeBihan D (1994) MR diffusion tensor spectroscopy and imaging. Biophys J 66:259–267.

Bellgowan PSF, Bandettini PA, van Gelderen P, Martin A, Bodurka J (2006) Improved BOLD detection in the medial temporal region using parallel imaging and voxel volume reduction. NeuroImage 29:1244–1251.

Bohsali AA, Triplett W, Sudhyadhom A, Gullett JM, McGregor K, FitzGerald DB, Mareci T, White K, Crosson B (2015) Broca's area–thalamic connectivity. Brain Lang 141:80-88.

Carlén M (2017) What constitutes the prefrontal cortex? Science 358:478–482.

Casas-Torremocha D, Porrero C, Rodriguez-Moreno J, García-Amado M, Lübke JHR, Núñez Á, Clascá F (2019) Posterior thalamic nucleus axon terminals have different structure and functional impact in the motor and somatosensory vibrissal cortices. Brain Struct Funct 224:1627–1645.

Cavada C, Compañy T, Tejedor J, Cruz-Rizzolo RJ, Reinoso-Suárez F (2000) The anatomical connections of the macaque monkey orbitofrontal cortex. A review. Cereb Cortex 10:220–242.

Clascá F (2022) Thalamic output pathways. In: The thalamus, pp 45–70. Cambridge, UK: Cambridge University Press.

Eradath MK, Pinsk MA, Kastner S (2021) A causal role for the pulvinar in coordinating task-independent cortico-cortical interactions. J Comp Neurol 529:3772–3784.

Erickson SL, Lewis DA (2004) Cortical connections of the lateral mediodorsal thalamus in cynomolgus monkeys. J Comp Neurol 473:107–127.

Euston DR, Gruber AJ, McNaughton BL (2012) The role of medial prefrontal cortex in memory and decision making. Neuron 76:1057-1070.

Farrell JAD, Landman BA, Jones CK, Smith SA, Prince JL, van Zijl PCM, Mori S (2007) Effects of signal-to-noise ratio on the accuracy and reproducibility of diffusion tensor imaging–derived fractional anisotropy, mean diffusivity, and principal eigenvector measurements at 1.5T. J Magn Reson Imaging 26:756–767.

Frey S, Mackey S, Petrides M (2014) Cortico-cortical connections of areas 44 and 45B in the macaque monkey. Brain Lang 131:36-55.

Giguere M, Goldman-Rakic PS (1988) Mediodorsal nucleus: areal, laminar, and tangential distribution of afferents and efferents in the frontal lobe of rhesus monkeys. J Comp Neurol 277:195–213.

Gilbert SJ, Spengler S, Simons JS, Steele JD, Lawrie SM, Frith CD, Burgess PW (2006a) Functional specialization within rostral prefrontal cortex (area 10): a meta-analysis. J Cogn Neurosci 18:932-948.

Gilbert SJ, Spengler S, Simons JS, Frith CD, Burgess PW (2006b) Differential functions of lateral and medial rostral prefrontal cortex (area 10) revealed by brain–behavior associations. Cereb Cortex 16:1783-1789.

Giraldo-Chica M, Rogers BP, Damon SM, Landman BA, Woodward ND (2018) Prefrontal-thalamic anatomical connectivity and executive cognitive function in schizophrenia. Biol Psychiatry 83:509–517.

Glasser MF, Coalson TS, Robinson EC, Hacker CD, Harwell J, Yacoub E, Ugurbil K, Andersson J, Beckmann CF, Jenkinson M, Smith SM, Van Essen DC (2016) A multi-modal parcellation of human cerebral cortex. Nature 536:171–178.

Goldman-Rakic PS, Porrino LJ (1985) The primate mediodorsal (MD) nucleus and its projection to the frontal lobe. J Comp Neurol 242:535–560.

Groenewegen HJ (1988) Organization of the afferent connections of the mediodorsal thalamic nucleus in the rat, related to the mediodorsal-prefrontal topography. Neurosci 24: 379–431.

Groh A, Bokor H, Mease RA, Plattner VM, Hangya B, Stroh A, Deschenes M, Acsády L (2014) Convergence of cortical and sensory driver inputs on single thalamocortical cells. Cereb Cortex 24:3167–3179.

Guillery RW, (1995) Anatomical evidence concerning the role of the thalamus in corticocortical communication: a brief review. J Anat 187 (Pt 3):583–592.

Halassa MM, Kastner S (2017) Thalamic functions in distributed cognitive control. Nat Neurosci 20:1669–1679.

Hirai T, Jones EG (1989) A new parcellation of the human thalamus on the basis of histochemical staining. Brain Res Brain Res Rev 14:1–34.

Iglesias JE, Insausti R, Lerma-Usabiaga G, Bocchetta M, Van Leemput K, Greve DN, van der Kouwe A, Fischl B, Caballero-Gaudes C, Paz-Alonso PM (2018) A probabilistic atlas of the human thalamic nuclei combining ex vivo MRI and histology. NeuroImage 183:314–326.

Inase M, Tokuno H, Nambu A, Akazawa T, Takada M (1996) Origin of thalamocortical projections to the presupplementary motor area (pre-SMA) in the macaque monkey. Neurosci Res 25:217–227.

Jenkinson M, Beckmann CF, Behrens TEJ, Woolrich MW, Smith SM (2012) FSL. NeuroImage 62:782–790.

Jeurissen B, Tournier JD, Dhollander T, Connelly A, Sijbers J (2014) Multi-tissue constrained spherical deconvolution for improved analysis of multi-shell diffusion MRI data. NeuroImage 103:411–426.

Kellner E, Dhital B, Kiselev VG, Reisert M (2016) Gibbs-ringing artifact removal based on local subvoxel-shifts. Magn Reson Med 76:1574–1581.

Kito S, Jung J, Kobayashi T, Koga Y (2009) Fiber tracking of white matter integrity connecting the mediodorsal nucleus of the thalamus and the prefrontal cortex in schizophrenia: A diffusion tensor imaging study. Eur Psychiatry 24:269–274.

Klein JC, Rushworth MFS, Behrens TEJ, Mackay CE, de Crespigny AJ, D'Arceuil H, Johansen-Berg H (2010) Topography of connections between human prefrontal cortex and mediodorsal thalamus studied with diffusion tractography. NeuroImage 51:555–564.

Kuramoto E, Pan S, Furuta T, Tanaka YR, Iwai H, Yamanaka A, Ohno S, Kaneko T, Goto T, Hioki H (2017) Individual mediodorsal thalamic neurons project to multiple areas of the rat prefrontal cortex: A single neuron-tracing study using virus vectors. J Comp Neurol 525:166–185.

Lerma-Usabiaga G, Liu M, Paz-Alonso PM, Wandell BA (2023) Reproducible Tract Profiles 2 (RTP2) suite, from diffusion MRI acquisition to clinical practice and research. Sci Rep 13:6010.

Li K, Fan L, Cui Y, Wei X, He Y, Yang J, Lu Y, Li W, Shi W, Cao L, Cheng L, Li A, You B, Jiang T (2022) The human mediodorsal thalamus: Organization, connectivity, and function. NeuroImage 249:118876.

Liu M, Lerma-Usabiaga G, Clascá F, Paz-Alonso PM (2022) Reproducible protocol to obtain and measure first-order relay human thalamic white-matter tracts. NeuroImage 262:119558.

Long Z, Xu Q, Miao H-H, Yu Y, Ding M-P, Chen H, Liu Z-R, Liao W (2017) Thalamocortical dysconnectivity in paroxysmal kinesigenic dyskinesia: Combining functional magnetic resonance imaging and diffusion tensor imaging: Thalamocortical Dysconnectivity In PKD. Mov Disord 32:592–600.

McFarland NR, Haber SN (2002) Thalamic relay nuclei of the basal ganglia form both reciprocal and nonreciprocal cortical connections, linking multiple frontal cortical areas. J Neurosci 22:8117-32.

Maguire EA, Frith CD, Morris RGM (1999) The functional neuroanatomy of comprehension and memory: The importance of prior knowledge. Brain 122:1839–1850.

Mátyás F, Lee J, Shin HS, Acsady L (2014) The fear circuit of the mouse forebrain: connections between the mediodorsal thalamus, frontal cortices and basolateral amygdala. Eur J Neurosci 39: 1810–1823.

Morel A, Liu J, Wannier T, Jeanmonod D, Rouiller EM (2005) Divergence and convergence of thalamocortical projections to premotor and supplementary motor cortex: a multiple tracing study in the macaque monkey. Eur J Neurosci 21:1007–1029.

Mori S, Crain BJ, Chacko VP, van Zijl PC (1999) Three-dimensional tracking of axonal projections in the brain by magnetic resonance imaging. Ann Neurol 45:265–269.

Nieuwenhuys, R. (2013) The myeloarchitectonic studies on the human cerebral cortex of the Vogt–Vogt school, and their significance for the interpretation of functional neuroimaging data. Brain Struct Funct 218:303–352.

Nieuwenhuys R, Voogd J, Van Huijzen C (2008) The human central nervous system. Berlin, Heidelberg: Springer.

Parnaudeau S, O'Neill P-K, Bolkan SS, Ward RD, Abbas AI, Roth BL, Balsam PD, Gordon JA, Kellendonk C (2013) Inhibition of mediodorsal thalamus disrupts thalamofrontal connectivity and cognition. Neuron 77:1151–1162.

Petrides M, Pandya DN (1984) Projections to the frontal cortex from the posterior parietal region in the rhesus monkey. J Comp Neurol 228:105–116.

Petrides M, Pandya DN (2009) Distinct parietal and temporal pathways to the homologues of Broca's area in the monkey. PLoS Biol 7:e1000170.

Petrides M, Tomaiuolo F, Yeterian EH, Pandya DN (2012) The prefrontal cortex: Comparative architectonic organization in the human and the macaque monkey brains. Cortex 48:46–57.

Porrino LJ, Crane AM, Goldman-Rakic PS (1981) Direct and indirect pathways from the amygdala to the frontal lobe in rhesus monkeys. J Comp Neurol 198: 121–136.

Preuss TM, Goldman-Rakic PS (1987) Crossed corticothalamic and thalamocortical connections of macaque prefrontal cortex. J Comp Neurol 257:269–281.

Preuss TM, Wise SP. (2021) Evolution of prefrontal cortex. Neuropsychopharmacology. 47:3-19.

Ray JP, Price JL (1993) The organization of projections from the mediodorsal nucleus of the thalamus to orbital and medial prefrontal cortex in macaque monkeys. J Comp Neurol 337:1–31.

Rodriguez-Moreno J, Porrero C, Rollenhagen A, Rubio-Teves M, Casas-Torremocha D, Alonso-Nanclares L, Yakoubi R, Santuy A, Merchan-Pérez A, DeFelipe J, Lübke JHR, Clasca

F (2020) Area-specific synapse structure in branched posterior nucleus axons reveals a new level of complexity in thalamocortical networks. J Neurosci 40:2663–2679.

Romanski LM, Giguere M, Bates JF, Goldman-Rakic PS (1997) Topographic organization of medial pulvinar connections with the prefrontal cortex in the rhesus monkey. J Comp Neurol 379: 313-32.

Rudebeck PH, Rich EL (2018) Orbitofrontal cortex. Curr Biol 28:R1083-R1088.

Saalmann YB, Pinsk MA, Wang L, Li X, Kastner S (2012) The pulvinar regulates information transmission between cortical areas based on attention demands. Science 337:753–756.

Salami M, Itami C, Tsumoto T, Kimura F (2003) Change of conduction velocity by regional myelination yields constant latency irrespective of distance between thalamus and cortex. Proc Natl Acad Sci U S A 100:6174–6179.

Saygin ZM, Kliemann D, Iglesias JE, van der Kouwe AJW, Boyd E, Reuter M, Stevens A, Van Leemput K, McKee A, Frosch MP, Fischl B, Augustinack JC, Alzheimer's Disease Neuroimaging Initiative (2017) High-resolution magnetic resonance imaging reveals nuclei of the human amygdala: manual segmentation to automatic atlas. Neuroimage 155:370–382.

Schilling KG et al. (2021) Tractography dissection variability: What happens when 42 groups dissect 14 white matter bundles on the same dataset? NeuroImage 243:118502.

Schmahmann JD, Pandya DN (2009) Fiber pathways of the brain. Cambridge, UK: Oxford University Press.

Schmitt LI, Wimmer RD, Nakajima M, Happ M, Mofakham S, Halassa MM (2017) Thalamic amplification of cortical connectivity sustains attentional control. Nature 545:219–223.

Schofield BR, Schofield RM, Sorensen KA, Motts SD (2007) On the use of retrograde tracers for identification of axon collaterals with multiple fluorescent retrograde tracers. Neuroscience 146:773–783.

Sherman SM, Guillery RW (1996) Functional organization of thalamocortical relays. J Neurophysiol 76:1367–1395.

Sherman SM, Guillery RW (2002) The role of the thalamus in the flow of information to the cortex. Phil Trans R Soc Lond B Biol Sci 357:1695–1708.

Siwek DF, Pandya DN (1991) Prefrontal projections to the mediodorsal nucleus of the thalamus in the rhesus monkey. J Comp Neurol 312:509–524.

Smaers JB, Gómez-Robles A, Parks AN, Sherwood CC (2017) Exceptional evolutionary expansion of prefrontal cortex in great apes and humans. Curr Biol. 27:714-720.

Smith SM, Jenkinson M, Woolrich MW, Beckmann CF, Behrens TEJ, Johansen-Berg H, Bannister PR, De Luca M, Drobnjak I, Flitney DE, Niazy RK, Saunders J, Vickers J, Zhang Y, De Stefano N, Brady JM, Matthews PM (2004) Advances in functional and structural MR image analysis and implementation as FSL. NeuroImage 23:208–219.

Theyel BB, Llano DA, Sherman SM (2010) The corticothalamocortical circuit drives higher-order cortex in the mouse. Nat Neurosci 13:84–88.

Tournier JD, Calamante F, Connelly A (2010) Improved probabilistic streamlines tractography by 2nd order integration over fibre orientation distributions. Paper presented at 2010 ISMRM, Stockholm, Sweden, May.

Tournier JD, Smith R, Raffelt D, Tabbara R, Dhollander T, Pietsch M, Christiaens D, Jeurissen B, Yeh CH, Connelly A (2019) MRtrix3: A fast, flexible and open software framework for medical image processing and visualisation. NeuroImage 202:116137.

Veraart J, Novikov DS, Christiaens D, Ades-aron B, Sijbers J, Fieremans E (2016) Denoising of diffusion MRI using random matrix theory. NeuroImage 142:394–406.

Virtanen P et al. (2020) SciPy 1.0: fundamental algorithms for scientific computing in Python. Nat Methods 17:261–272.

Warren JM, Akert K (1964) The frontal granular cortex and behavior. New York, NY: McGraw-Hill.

Yeterian EH, Pandya DN (1991) Prefrontostriatal connections in relation to cortical architectonic organization in rhesus monkeys. J Comp Neurol 312:43–67.

Zhang F, Wu Y, Norton I, Rathi Y, Golby AJ, O'Donnell LJ (2019) Test–retest reproducibility of white matter parcellation using diffusion MRI tractography fiber clustering. Hum Brain Mapp 40:3041–3057.